Dual targeting of mitochondrial Lon peptidase 1 and chymotrypsin-like protease by small molecule BT317, as potential therapeutics in malignant astrocytoma

Christopher Douglas[1¥], Shashi Jain[2¥], Naomi Lomeli[2], Kaijun Di[2], Nitesh Kumar Nandwana[5], Adil Shareef Mohammed[5], Thao Vu[2], James Pham[2], Javier Lepe[1], Maria Cristina Kenney[3], Bhaskar Das[4,5]* and Daniela A. Bota[1,2,6]*

[1] Department of Pathology & Laboratory Medicine, University of California Irvine, Irvine, CA, USA (C.D., D.A.B.)
[2] Department of Neurology, University of California Irvine, Irvine, CA, USA (S.J., K.D., N.L., T.V., J.P.)
[3] Department of Ophthalmology Research, University of California Irvine, Irvine, CA, USA (M.C.K.)
[4] Arnold & Marie Schwartz College of Pharmacy & Health Sciences, Long Island University – Brooklyn, NY, USA (N.K.D, B.D.)
[5] Department of Pharmacology, Long Island University – Brooklyn, NY, USA (B.D.)
[6] Chao Family Comprehensive Cancer Center, University of California Irvine, Irvine, CA, USA (D.A.B.)
¥ These authors contributed equally.
* Correspondence: Email: dbota@hs.uci.edu, Phone: (949) 824-7377, Fax: 714-456-6894 (Daniela A. Bota, M.D., Ph.D.); E-mail: Bhaskar.Das@liu.edu Phone: (718) 488-1471, Fax: 718-780-4586, Bhaskar Das, Ph.D.

Simple Summary: We demonstrate here that BT317 has activity in patients derived malignant astrocytomas models by dual inhibiting mitochondrial Lon Peptidase I (LonP1) and the Chymotrypsin-Like (CT-L) proteasome activity. Malignant astrocytomas (including both IDH mutant astrocytomas grade 4 and IDH wildtype glioblastoma) have poor clinical outcomes, and novel treatments are needed to limit recurrence and improve overall survival. These tumors have a malignant phenotype that is mediated by altered mitochondrial metabolism, abnormal protein processing, and adaptation to hypoxia. We have previously published that gliomas are especially vulnerable to proteasome inhibitors as well as to inhibitors of the mitochondrial Lon Peptidase I (LonP1), but the effect of combining the two strategies has not been reported. Here, we present evidence dual inhibition of LonP1 and Chymotrypsin-like (CT-L) proteasome activity with the small-molecule BT317 can effectively induce cellular reactive oxygen species (ROS) production leading to apoptosis in clinically relevant malignant astrocytoma patient-derived orthotopic models. BT317 showed strong synergy with the standard of care, temozolomide (TMZ), in the astrocytoma models independent of their IDH profile. This preclinical study demonstrated a potential dual LonP1 and CT-L proteasome inhibitor as novel therapeutic strategies for malignant astrocytoma and provided insight for future clinical translation studies alone or in combination with the standard of care.

Abstract: Malignant astrocytomas are aggressive glioma tumors characterized by extensive hypoxia-induced, mitochondria-dependent changes such as altered respiration, increased chymotrypsin-like (CT-L) proteasome activity, decreased apoptosis, drug resistance, stemness and increased invasiveness. Mitochondrial Lon Peptidase I (LonP1) overexpression and increased CT-L proteasome inhibitors activity are the biomarkers of aggressive high grade glioma phenotype, poor prognosis and found to be associated with recurrence and poor patient survival, and drugs targeting either LonP1 or the CT-L activity have anti-glioma activity in preclinical models. We here for the first time introduced and evaluated a novel small molecule, BT317, derived from coumarinic compound 4 (CC4) using structure-activity modeling which we found to inhibit both LonP1 and CT-L proteasome activity. Using gain-of-function and loss-of-function genetic models, we discovered that BT317 is more effective than the individual LonP1 or CT-L inhibition in increasing reactive oxygen species (ROS) generation and inducing apoptosis in high-grade astrocytoma lines. *In vitro*, BT317 had activity as a single agent but, more importantly, enhanced synergy with the standard of care commonly used chemotherapeutic temozolomide (TMZ). In orthotopic xenograft, patient derived glioma models, BT317 was able to cross the blood-brain barrier, to show selective activity at the tumor site and to demonstrate therapeutic efficacy both as a single agent and in combination with TMZ. BT317 defines an emerging class of dual LonP1, and CT-L proteasome inhibitors exhibited promising anti-tumor activity and could be a promising candidate for clinical translation in the space of malignant astrocytoma therapeutics.

Keywords: malignant astrocytoma; Glioblastoma; LonP1; CT-L proteasome; BT317, reactive oxygen species

Graphical Abstract:

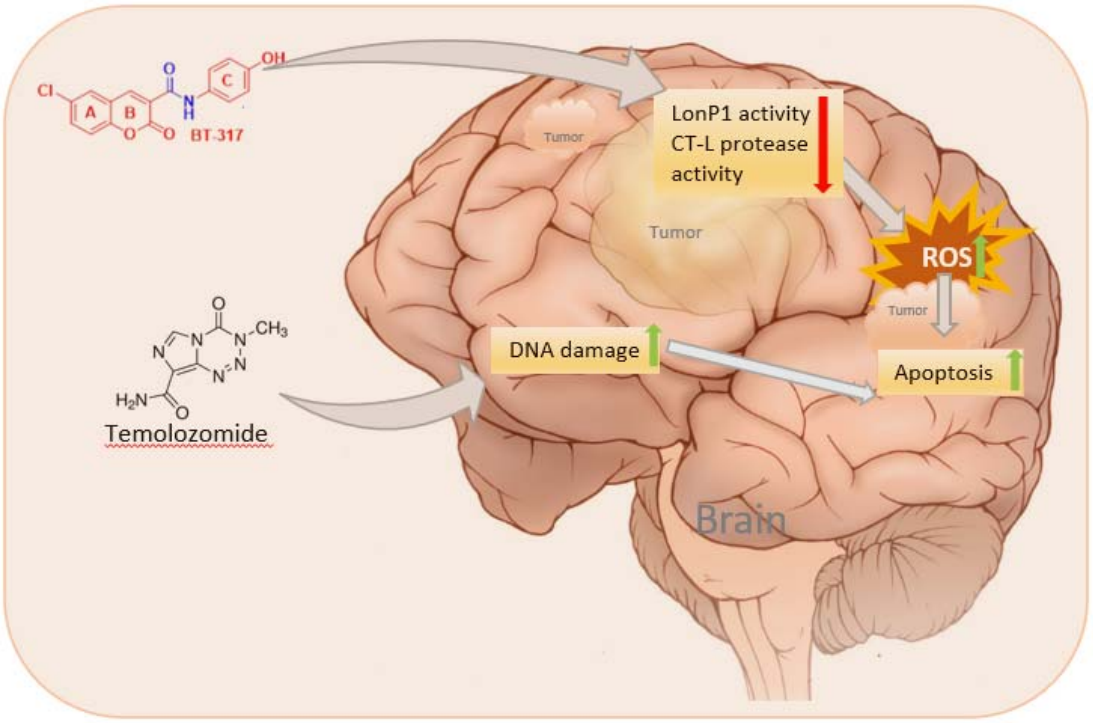

Highlights

1. The novel compound BT317 acts as a dual inhibitor of LonP1 and chymotrypsin-like proteasome enzymatic activity.
2. LonP1 and CT-L proteasome inhibition by BT317 drives ROS production in malignant astrocytoma independent of genetic profile.
3. LonP1 and CT-L proteasome inhibition drives autophagy in IDH mutant astrocytoma.
4. BT317 shows blood-brain barrier permeability and has low normal tissue toxicity.
5. BT317 synergizes with the first-line chemotherapy agent Temozolomide (TMZ).

1. Introduction

Malignant astrocytomas are the most aggressive brain tumors, with a less than three-year expected survival rate following surgical resection, radiation, and chemotherapy. The current standard of care, temozolomide (TMZ, temodar), an alkylating agent, provides a median survival advantage of 2.5 months when added to surgery and radiation therapy[3]. The use of Tumor-Treating Fields (TTFields, Optune) further increases this survival advantage by 4 months[4]. Despite significant efforts and numerous past and ongoing clinical trials utilizing small molecule inhibitors such as the STAT3 inhibitor WP1066, EGFR inhibitors, Dopamine Receptor D2 antagonists (ONC201), and immunotherapy checkpoint inhibitor approaches such as pembrolizumab, nivolumab and ipilimumab, the development of safe and efficacious therapies for malignant astrocytomas has been slow and still under evaluation. In the past 16 years, only three therapies (TMZ, bevacizumab, TTFields) have been approved for the treatment of astrocytomas[5]. Thus, there is an urgent need to develop alternative therapeutic strategies.

Malignant astrocytomas are currently classified based on their genetic and epigenetic profiles like isocitrate dehydrogenase 1 or 2 (IDH1/2) mutant/wildtype, ATRX (retention/loss), and p53 (mutant/wildtype)[6]{Hegi, 2005 #109;Hegi, 2005 #1}. Less than 10% of grade 4 astrocytomas express IDH mutations, which are associated with an improved response to treatment and prognosis as compared with the IDH wildtype tumors[7]. Based on these biologic and survival differences, the most recent WHO glioma classification excludes tumors with an IDH mutation from being classified as GBM and refers to such tumors as astrocytoma grade 4, IDH mutant[8]. Even though the presence of the IDH mutations predict a better outcome, the survival of patients with grade 4 IDH mutated astrocytoma treated with the standard therapy (radiation and TMZ) is still only 31 months[9] as compared with the GBM patients with a wildtype IDH status which survive in average less than 24 months [4]. The presence of the IDH mutation (>90% are IDH1-R132H) can drive tumorigenesis[10] at the cost of impairing the mitochondrial electron transport chain in cellular mitochondria, increasing ROS production, and creating increased vulnerability to pro-oxidative and apoptotic signals[11]. Due to the differences in the genetic profile, response to treatment and overall survival, it is imperative to include both types of malignant astrocytoma models in the efforts to develop novel therapies.

The invasive phenotype of malignant astrocytomas is partly mediated by overexpression of the transcriptional activator hypoxia-inducible factor 1 alpha (HIF-1α). HIF-1α contributes to the hypoxia-driven maintenance of glioma stem cells (GSCs)[12] by supporting self-renewal[13], angiogenesis[14], increased invasiveness[15], and high levels of genetic instability. The latter contributes to

tumor heterogeneity and presents a major challenge in devising novel therapeutic strategies for its treatment[16]. There are hundreds of gene targets in the HIF-1α signaling pathway and the nuclear-encoded Lon Peptidase 1 (LonP1) is directly upregulated by HIF-1α[17]. LonP1 protease degrades aconitase. Aconitase plays a role in the TCA cycle by converting isocitrate to citrate, which is a metabolite used by isocitrate dehydrogenase (IDH) to produce alpha-ketoglutarate. LonP1 is an ATP-dependent protease that regulates mitochondrial homeostasis through three main functions: (1) proteolytic degradation of mitochondrial proteins[17], (2) protein chaperone[18], and (3) mitochondrial DNA (mtDNA)-binding protein[19]. LonP1 overexpression is a poor prognostic factor that is known to promote invasion and metastasis in multiple cancers, including colorectal[20], melanoma[20] and oral cancer[21]. Our previous results showed that LonP1 is overexpressed in astrocytomas, and its elevated expression levels are associated with high tumor grade and poor survival[22]. Furthermore, LonP1 knockdown in established human glioma lines, D-54 MG and U-251 MG, reduced cell viability under normal conditions, and drastically impaired survival under hypoxic conditions[22]. This is concomitant with a decrease in mitochondrial respiration. On the contrary, there are established studies stating differentiated astrocytomas tumor cells are more glycolytic while GSCs are more dependent on mitochondria biogenesis [23,24]. Notably, LonP1 pharmacological inhibition using the coumarinic compound 4 (CC4)[25] inhibited glioma cell proliferation and synergistically enhanced the therapeutic efficacy of TMZ, *in vitro*[22].

There is difficulty in the generation of specific LonP1 inhibitors[25], which is attributable to its structural similarities with other known proteases and the proteasome[26]. However, targeting specifically the chymotrypsin-like (CT-L) proteasome activity may be beneficial, as it plays an important role in tumor cell survival[27] and treatment resistance[28]. Dual inhibition of LonP1 and the CT-L proteasome activity could be potentially beneficial as it could offer additional therapeutic benefits compared with targeting either protease activity alone. Recent work in multiple myeloma has demonstrated the strong synergy with LonP1 and CT-L proteasome inhibition[29], using specific inhibitors previously shown to have no cross activity, and to target only LonP1, Bardoxolone methyl (CDDO-ME)[30,31], and the CT-L proteasome activity, carfilzomib (CFZ)[32]. Bortezomib (BTZ) exhibits dual LonP1 and CT-L inhibition and possesses a boronic acid group that can transform into a boronate ester when exposed to reactive oxygen species (ROS)[33]; however, the major limitation is its poor blood-brain barrier (BBB) permeability[34]. In the subcutaneous U-87 MG and U-251 MG glioma models, BTZ was found to sensitize the glioma tumors to TMZ by suppressing FOXM1-mediated treatment resistance[35]. Another limitation with the study was that they did not use patient-derived lines and resorted to using a subcutaneous model instead of an orthotopic xenograft model. In a cell-based high content screen of the compounds synthesized, we identified BT317, a derivative of CC4[22,25] and a dual LonP1 protease and CT-L proteasome inhibitor as agents with selective anticancer activity. In this study, we assessed its LonP1 protease and proteasome inhibition profiles. We then investigated the efficacy and feasibility of BT317 as a single agent and in combination with TMZ as a therapeutic strategy for malignant astrocytomas, including patient-derived, orthotopic xenograft models. We have selected patient derived astrocytoma lines with all possible combination of genetic and epigenetic profiles like isocitrate dehydrogenase 1 or 2 (IDH1/2) mutant/wildtype, ATRX (retention/loss), and p53 (mutant/wildtype) to identify if BT317 targets a specific astrocytoma subtype.

2. Methods

2.1. Ethics Statement

All astrocytoma tumor specimens were collected under institutional review board approved protocols from patients who underwent surgical tumor resection at the University of California Irvine Medical Center. The neuropathological review was completed by a specialized neuropathologist. All patient-derived samples were deidentified. All animal studies were performed in accordance with the guidelines established by the Institutional Animal Care and Use Committee (IACUC) at the University of California Irvine.

2.2. Synthesis of small molecule BT317 and related compounds

Synthesis of BT317 was initiated using compound **D** (methyl 6-chloro-2-oxo-2H-chromene-3-carboxylate) (**Fig. 1A**). Compound **D** was then synthesized from Compound **A** using the outlined process by first adding 5-chlorosalicyclaldehyde (A, 1.55 g, 10 mM) to CH_3CN (5 mL) in a 35 mL reaction tube. Dimethylmalonate (**B**) (1.45 g, 11 mM) and ethyl piperdine-3-carboxylate (**C**) (15 mg, 10 mol%) in 15 mL of CH_3CN were added. The resulting reaction mixture was stirred at room temperature for 24 h. After the evaporation of CH_3CN, the crude reaction mixture was purified by silica gel chromatography to give a white solid **D** (1.6 g, 60%). Basic hydrolysis of compound **D** was performed to produce Compound **E** acid (6-chloro-2-oxo-2H-chromene-3-carboxylic acid). Acid synthesis was initiated by adding methyl 6-chloro-2-oxo-2H-chromene-3-carboxylate D (1.0 g, 4.2 mM) in ethanol to sodium hydroxide (10% w/v in 20 mL ethanol). The mixture was stirred under reflux for 24 h. After the completion of the reaction, the mixture was cooled to room temperature and diluted with 10% HCl. The solid precipitated out and was isolated and washed with water, yielding compound **E** (white solid, 80% yield). Using compound **E**, we further derivatized to amide (BT173) using a simple amide coupling reaction in the presence of coupling reagents. The 6-chloro-2-oxo-2H-chromene-3-carboxylic acid **E** (1.0 mM) was dissolved in dichloromethane (DCM) (3 mL) in a 35 mL reaction tube. Then 4-hydroxy aniline (1.1 mM) and DCC (1.2 mM) were added. The resulting reaction mixture was stirred at room temperature for 24 h. The reaction was then quenched with a saturated aqueous NaOH solution and extracted with DCM (10 × 3 mL). The combined organic layers were dried over Na_2SO_4 and then filtered. After evaporation of the organic solvent, the residue was purified by silica gel chromatography to obtain BT317, 6-Chloro-N-(4-hydroxyphenyl)-2-oxo-2H-chromene-3-carboxamide (**Fig. 1B;** white solid, 78% yield). The reagents used for the synthesis were purchased from Fisher Scientific. The structure was confirmed by nuclear magnetic resonance (NMR) and proton,

carbon, and mass spectrometry, and the purity of the compound was determined by HPLC. The lead compound, BT317, was evaluated using NMR as follows: 1H NMR (500 MHz, DMSO-d6) δ 10.44 (s, 1H), 9.43 (s, 1H), 8.87 (s, 1H), 8.16 (d, J = 2.5 Hz, 1H), 7.82 (dd, J = 8.8, 2.6 Hz, 1H), 7.61 (d, J = 8.9 Hz, 1H), 7.53 (d, J = 8.5 Hz, 2H), 6.78 (d, J = 8.4 Hz, 2H). 13C NMR (125 MHz, DMSO) δ 160.0, 158.8, 154.2, 152.4, 145.7, 134.2, 133.5, 129.5, 129.0, 121.6, 121.2, 119.9, 118.2, 115.3. HRMS (ESI) was calculated for $C_{16}H_{11}ClNO_4$ (M.W. = 316.0371) and 316.0607 [M + H]+.

2.3. Primary and Established Cell Lines

2.3.1. Primary Glioma/Astrocytoma Stem Cell Cultures (GSC)

Patient-derived GSC were isolated from surgical astrocytoma samples in the laboratory of Dr. Daniela A. Bota (DAB), using a previously established method[36]. All GSC cultures were maintained as non-adherent neurospheres in Neurobasal medium (Thermo Fisher; 12349015) supplemented with 20 µg/mL EGF (Thermo Fisher; PHG0313), 20 µg/mL FGF (Thermo Fisher; PHG0023), B27 (Life Technologies; 12587010), GlutaMAX (Thermo Fisher; 35050061), 5 mM sodium pyruvate (Thermo Fisher; 11360070), and antibiotics (Thermo Fisher; 15070063, 15290018). The patient derived GSC lines included DB70, DB76, DB77, DB81, and 83MES. The patient-derived 83MES line was a kind gift from Dr. Ichiro Nakano at the University of Alabama at Birmingham. Each cell line was expanded, cryopreserved as low-passage stocks, and tested for mycoplasma using a MycoScope PCR Mycoplasma Detection Kit (Genlantis, MY01050). All the cell lines were used for the initial 10 passages.

2.3.2. Established Human Glioma Cell Lines

Five established human glioma cell lines, U-251 MG, D-54 MG, and U-87 MG, and the pediatric CHLA-200, were maintained in DMEM/F-12 medium (Corning; 10-090-CV) containing 292 µg/ml glutamine, 1% penicillin/streptomycin (Thermo Fisher; 15070063), and 10% FBS (Invitrogen; 10371-029). All the cell cultures were maintained at 37°C and 5% CO_2 in a humidified incubator.

2.3.3. Normal Cell Lines

The human mammary gland epithelial adherent non-tumorigenic cell line MCF-10A was maintained in DMEM/F-12 medium containing 0.5 mg/mL hydrocortisone, 20 ng/mL hEGF, 100 ng/mL cholera toxin, 1% penicillin/streptomycin, and 5% horse serum (Life Technologies; 26050-070). The human lung fibroblast line HPF242 was maintained in DMEM/F-12 containing 10% FBS and 1% penicillin/streptomycin. All the cell cultures were maintained at 37°C and 5% CO_2 in a humidified incubator. Unlisted reagents were purchased from Sigma-Aldrich and Thermo Fisher Scientific.

2.3.4. Generation of Transgenic Patient-derived Glioma Stem Cells

The LonP1 overexpressing and vector control clones were made by transfecting DB70, DB76, DB77 and MES83 cells with lentivirus-encoding human LonP1, cloned into the vector pLVX-EF1α (Takara Biosciences, Nojihigashi, Japan, #631982), and sorted to 100% purity by FACS following ZsGreen1 expression with a BD FACSAria II cell sorter. A virus containing the empty pLVX construct was used as control. Also, the doxycycline inducible 3 unique shRNAs LONP1-Human clones were prepared from 29mer shRNA constructs in lentiviral GFP vector pGFP-C-shLenti (Origene: TR30023) (Gene ID = 9361) along with 29-mer scrambled shRNA cassette in pGFP-C-shLenti Vector, TR30021, obtained from Origene. The LonP1 knockdown and scrambled clones were made by transfecting DB70, DB76, DB77 and MES83.

2.4. XTT Viability Assay

All established and patient-derived astrocytoma cell lines were seeded at a density of 10,000 cells per well in a 96-well plate (n = 4 replicates per condition). The following day, equal volumes of synthesized inhibitors dissolved in DMSO were added to each well at the specified concentrations (0.1-1000 µM). For the synergy experiments, BT317 was added at specified concentrations with a fixed and specified TMZ concentration. After 5days, 25 µL of XTT Cell Viability Assay solution (Biotium, 30007) was added. After 4 h, the absorbance was measured at 490 nm using a SpectraMax Plus 384 microplate reader. GraphPad was then used to perform a log transformation and generate a nonlinear regression curve to calculate IC_{50} viability. The Biochemically Intuitive Generalized Loewe Model (BIGL) was used to determine agonism or antagonism (https://cran.r-project.org/web/packages/BIGL)[37].

2.5 Apoptosis Analysis by Flow Cytometry

Patient derived DB70 and DB77 cells (10^5 per condition) were treated with CDDO-ME and CFZ alone or in combination as stated in figure. Five days later, all the cells were collected, washed with DPBS and stained with propidium iodide (PI, Sigma, P4864) staining solution containing 50 µg/ml PI, and 100 µg/ml DNase-free RNaseA, and incubated for 5 minutes at room temperature. At the end of the incubation time, the cells were subjected to fluorescence-activated cell analysis of DNA content. The percentage of cells with sub diploid DNA content was taken as a measure of the apoptotic rate of the cell population. Flow cytometry was performed on a BD Fortessa X-20 (BD) analyzer, and the data were analyzed using FlowJo (Treestar) software.

2.5. Reactive Oxygen Species Assay

The DB70 line was plated and incubated for 12 h prior to starting treatment. CellROX™ Orange Reagent (Thermo Fisher, C10443) was then added at a working concentration of 5 µM for 30 minutes. After several 1X PBS washes, the cell samples were replated and then imaged using a 20X objective on a Keyence BZ-X810 Widefield Microscope.

2.6. Sphere formation assay

After exposure to doxycycline in indicated cells for 96 h, the cells were washed with HBSS and incubated with Accutase (Sigma, SCR005) for 3 min at 37 °C to create a single-cell suspension. Then, 1 mL of methylcellulose stock media was added (R&D Systems, HSC001) to a 24-well non-treated plate. Then, 1 mL of the indicated media containing 4000 cells were added. The cells were gently mixed by swirling with 200 pipette tips until got uniformly distributed without introducing bubbles in the well. After 14 days of incubation at 37°C incubator with humidity, images of tumor colonies were captured and quantified using ImageJ (NIH).

2.6. Western Blotting

Cell culture samples were exposed to indicated drug for mentioned period prior to lysis with RIPA lysis buffer containing 1 mM PMSF, 1 mM Na_3VO_4, and a protease inhibitor cocktail (Sigma, P8340-1ML). The protein concentration was standardized using the DC Protein Assay (Bio-Rad, 500-0114) with a SpectraMax Plus 384 microplate reader. A Precision Plus Protein Kaleidoscope™ ladder (Bio-Rad, 161-0375) and approximately 20 µg of sample were loaded onto each well and run on a Mini Protean TGX Gel (Bio-Rad, 456-1046) before being transferred to an Immobilon Transfer Membrane (Millipore, IPVH08130). The membranes were probed with the indicated primary antibodies and the appropriate secondary antibodies. The primary and secondary antibodies used were 1:2000 LonP1 (Proteintech, 15440-1-AP), 1:1000 Aconitase2 (Abcam, ab71440), 1:1000 LC3B (Cell Signaling Technology, 2775S), FOXM1 (Millipore Sigma, SAB1412254-100UG), C-MET (Fisher Scientific, MAB3729), TFAM (Fisher Scientific, PA5-80107) 1:2000 B-Actin (Novus Biologicals, NB600-501), 1:1000 p-AKT (Abcam, ab192623-100ul), 1:10,000 goat anti-mouse IgG F(ab')2 (Enzo Life Sciences, ADI-SAB-100-J), and 1:3,000 IgG (H+L) Goat anti-Rabbit HRP (Invitrogen, 32460); these were used according to the manufacturer's recommendations and diluted in TBST with 3% BSA. Chemiluminescence was visualized using Amersham™ ECL™ Prime western blotting Detection Reagent (GE Healthcare, RPN2232) and imaged using an Azure c600 Molecular Imager. ImageJ was used to align the bands, improve contrast (<20%), and normalize and quantify all bands.

2.7. Mitochondria Isolation

Patient derived DB70 glioblastoma cells were grown in neurobasal media supplemented with penicillin (100 units/ml) and streptomycin (100 µg/ml), Amphotericin B (2.5 µg/ml), EGF (20 ng/ml), FGF (20 ng/ml), B27 supplement (), L-Glutamine (2 mM) and sodium pyruvate (1 mM). The cultures were grown in a humidified incubator containing 19.9% O2 and 5% CO2 at 37 °C. For isolating mitochondria, we collected $1X10^9$ cells for each experiment. Human DB70 cells mitochondria were isolated as described in a homogenizing buffer (225 mM mannitol, 75 mM sucrose, 0.5 mM EDTA and 25 mM HEPES, pH 7.4). Cells were passed through 25-gauge needle with a 1 ml syringe for homogenization at a consistent speed of 10 stocks with 2 mins break for a total of 4-6 times, throughout on ice. The integrity of the homogenized cell can be checked under a light microscope. Multiple rounds of centrifugations at 600g for 5 mins were performed to pellet out the unbroken cells and nuclei, plasma membranes, lysosomes, microsomes and cytosol respectively. The supernatant from these steps were centrifuged at 10,000g for 10 mins to pellet crude mitochondria. This step is repeated twice in homogenizing buffer to remove any microsomal contamination. The crude mitochondrial pellet is suspended in 1% digitonin lysis buffer (1% digitonin, 20mM Tris-HCL, 50mM NaCl, and 0.1 mM EDTA). After incubation for 30 min on ice, the lysates were centrifuged at 17000g for 10 mins to collect mitochondrial lysate in the supernatant and frozen at −70 °C until used.

2.8. Lon protease purification using Immunoprecipitation

The LonP1 protease is further purified from mitochondrial lysate. The Pierce Crosslink IP Kit (cat numbre: 26147) method was used to capture the LonP1 antibody to Protein A/G Agarose magnetic resin and covalently immobilizing it to the support by crosslinking with disuccinmidyl suberate (DSS). The LonP1 antibody resin is then incubated with the mitochondrial lysate that contains the protein antigen of interest, allowing the antibody:antigen complex to form. After washing to remove nonbound (presumably undesired) components of the sample, the antigen is recovered by dissociation from the antibody with elution buffer supplied in the kit. The entire procedure is performed using a magnetic eppendoff stand, allowing solutions to be fully separated from the magnetic agarose resin upon brief incubation at magnetic eppendoff stand. Only antigen (LonP1 protease here) was eluted by this procedure, enabling it to be identified and further analyzed without interference from antibody fragments.

2.9. LonP1 Protease Activity Assay

Purified LonP1 protease activity is analyzed using a Pierce Fluorescent Protease Assay Kit (Thermo Scientific™, 23266). The mitochondrial isolation step is introduced to enrich the LonP1 fractions and further did the LonP1 immunoprecipitation with the A/G magnetic bead crosslinked LonP1 antibody from this total mitochondrial lysate. Purified 200 nM LonP1 or equivalent total mitochondrial lysate and 10 mM $MgCl_2$ was prepared in BupH™ Tris-buffered saline. LonP1 inhibitors or vehicle (DMSO) were then added, and the samples were incubated at 37°C for 1 h. Following this incubation, an equal volume of 0.04 mg/mL FITC-

casein (Thermo Scientific™, 23267), 4 mM or 2 µM ATP (Thermo Fisher, R0441), and 10 mM $MgCl_2$ was added prior to measurement using a Biotek Synergy HT plate reader. Digestion of fluorescein-labeled casein was assessed by measuring fluorescence with excitation and emission filters at 485 and 534 nm, respectively.

2.10. Proteasome Activity Assay

Proteolytic activity was assessed using a Proteasome-Glo™ assay system (Promega, G8531), comprising Proteasome-Glo™ Chymotrypsin-Like Assay (G8621), Proteasome-Glo™ Trypsin-Like Assay (G8621) and Proteasome-Glo™ Caspase-Like Assay (G8621). The assay was performed according to the manufacturer's instructions. Tissue samples were flash frozen and ground using a Dounce Homogenizer (Fisher, 50-194-5205). Samples were then harvested in ice-cold lysis buffer composed of 50 mM HEPES (pH 7.4), 250 mM sucrose, 5 mM $MgCl_2$, 0.5 mM DTT, and 40 mM KCl in deionized, sterile water. For D-54 MG, cells were seeded at a density of 200,000 cells per well onto a 6-well plate and subsequently exposed to LonP1 inhibitors (BT317, BT395, BT397, and BT399) at the specified concentrations and endpoints. The lysates were incubated on ice for 30 min and centrifuged at 14,000 rpm for 10 min at 4°C. The supernatants were collected and mixed 1:1 with stabilizing buffer composed of 40 mM HEPES (pH 8.0), 1 mM EDTA, and 20% glycerol in deionized, sterile water. The protein concentration was standardized using the DC Protein Assay (Bio-Rad, 500-0114) with a SpectraMax Plus 384 microplate reader. Samples were then diluted with ice-cold proteasome dilution buffer and plated in a black, clear, flat-bottom 96-well plate at a concentration of 8 µg protein in 50 µL/well (n = 3-4 replicates/sample). The plates were placed on a plate shaker at 300-500 rpm for 30 s, followed by incubation for 10-30 minutes incubation at room temperature. Luminescence was read using a Biotek Synergy HT plate reader.

2.11. BT317 and TMZ Administration and Maximum Tolerated Dose (MTD) Escalation

BT317 and TMZ was reconstituted in DMSO to create a concentrated stock prior to further dilution in 500 µL 1XPBS to generate the correct dosage for intraperitoneal injection (i.p.) in 10–14-week-old Rag1 KO immunodeficient mice (Jackson Laboratory, B6.129S7-*Rag1*$^{tm\,1Mom}$/J). Mice were monitored following injection, and the clinical score was determined based on activity, appearance, and body condition with a maximum score of 3, which is necessary to define the MTD[38]. Mass spectrometry was performed on flash-frozen brains and tail vein blood drawn by contract research organizations (Cyprotex and Biotechnology Innovation and Optimization Center) to determine BT317 levels.

2.12. Patient-derived Orthotopic Xenograft Model

The patient-derived lines DB70, DB76, DB77 and 83MES were seeded into 3-dimensional organoids using an established methodology[39]. Upon full expansion, the organoids were dissociated, and 1,000-10,000 cells were intracranially implanted into the right frontal lobe of 10–14-week-old Rag1 KO immunodeficient mice (Jackson Laboratory, B6.129S7-*Rag1*$^{tm\,1Mom}$/J). After 5 or 10 days, treatment was initiated as specified, with intraperitoneal (i.p.) injections every other day for a total of 5 doses over a span of 5 or 10 days as specified. Animals were observed daily and sacrificed upon observation of distress, including hemiparesis, obtundation, hunchback, or weight loss of 20% from the maximum weight achieved.

2.13. Quantitative Polymerase Chain Reaction Assay

For each cell line, growth conditions were standardized and ~500,000 cells were collected and flash frozen. Samples were then processed according to the Quick-RNA™ Miniprep Plus Kit (Zymo Research, R1057) specifications to prepare pure RNA samples. These were used to generate cDNA samples using a two-step reverse transcriptase and polymerase chain reaction with PerfeCTa SYBR Green Supermix and transcript appropriate primers. The primers used include: LONP1 (5'-ATGGAGGACGTCAAGAAACG-3', 5'- GACGCTGAAGCGGAAGTACTC-3') and Forward and reverse primers (Tfam: Forward 5′-AAGGGAATGGGAAAGGTAGA-3′/Reverse 5′-AACAGGACATGGAAAGCAGAT-3′; β-actin: Forward 5′-TGTGACGTTGACATCCGTAA-3′/Reverse 5'-GCTAGGAGCCAGAGCAGTAA-3'). After preparing master mixes samples were prepared in quadruplicate in a 96-well Reaction Microplates (Fisher Scientific, 4346907) and measured following a standard qtPCR protocol with a QuantStudio 7 Real-Time PCR System. Annealing temperature and length were optimized for each primer pair. Amplification was measured as fluorescence in quadruplicate replicates and analyzed using QuantStudio 7 software.

2.14. Statistical Analysis

Data were analyzed using Student's t-test or log-rank (Mantel-Cox) test when appropriate. Data are presented as mean ± standard error of the mean (SEM). Significance between groups is denoted by $*P < 0.05$, $**P < 0.01$, $***P < 0.001$. Data were analyzed using the GraphPad Prism 5.0 software (GraphPad Software, La Jolla, CA, USA). For the XTT viability assays, raw data were processed using a log transform and a dose-response inhibition nonlinear model to determine IC50 and standard error. The statistical significance of the Kaplan-Meier survival curve was verified using the Mantel-Cox log-rank test.

3. Results

3.1. Dual targeting using specific LonP1 and chymotrypsin-like protease inhibitor enhances cytotoxicity in malignant astrocytoma patient derived linesirrespective of the IDH status.

proteasome inhibition has emerged as a compelling concept in oncology in the past decade. It has been well established that proteasome inhibitors selectively kill cancer cells, and the strong clinical selective anti-tumor activity observed in various malignancies. Since then, several structurally and mechanistically distinct proteasome inhibitors have entered clinical development in oncology with limited success. Mitochondrial metabolism and response to free radical damage is extensively regulated by mitochondrial Lon protease, encoded by nuclear gene LONP1. A synthetic triterpenoid CDDO-Me is a specific inhibitor of this LonP1 protease without effect on the proteasome[30,31]. Carfilzomim is a proteasome inhibitor that is highly selective for chymotryptic activity of the proteasome and has no effect on the LonP1 enzymatic activity[32]. Previous findings suggested that both LonP1 and chymotrypsin-like (CT-L) proteasome are stress-response genes and dual inhibition may be an effective strategy for targeting cancer cells; however, the exact mechanism has not been validated yet.

Here, we demonstrated that the selective LonP1 inhibitor, CDDO-ME[30], and CT-L proteasome inhibitor, Carfilzomib (CFZ)[30,31], have strong synergy in reducing viability of multiple patient-derived malignant astrocytoma lines (**Fig. 1A and B**). We performed a baseline validation of LonP1 protease, autophagy marker LC3B and aconitase (Aco2 which is Lon protease subastrate) protein expression levels in all the malignant astrocytoma cell lines used in this study to correlate with the inhibitory effects of relevant drugs (**Supplementary Fig. S1A)**. Interestingly, patient-derived malignant astrocytoma lines were found sensitive to CDDO-ME doses as low as 200 nM CDDO-ME and with CFZ doses the sensitivity is as low as 1 nM (**Fig. 1A**). Since we used the two drugs in combination, our next goal was to check the mechanism of interaction between the drugs. The degree of combination between the drugs either defines synergistic or anatagonistic interaction which is calculated using a reference model. In our study model, the interactive analysis and visualization dose combination response data of CDDO-ME and CFZ showed that the two drugs work in synergy, where a significantly low does of each drug in combination is more effective then individual effector drug doses **(Fig. B**). XTT results confirmed that our patient-derived malignant astrocytoma cell lines are sensitive to the existing LonP1 and CT-L inhibitors. These results were further confirmed and validated through Annexin V CoraLite 488 and PI staining in flow cytometric assay (**Supplementary Fig. S1B)**. We found that all malignant astrocytoma patient-derived lines used in this study showed similar sensitivity to CDDO-ME and CFZ inhibitor in two different assay readouts. Since LonP1 inhibition with CDDO-ME was shown to induce oxidative stress that leads to autophagy mediated death in various human cancer cell lines[31], we also tested for the known autophagy markers LC3B-I. Our immunoblot results in DB70 line, upon CDDO-ME treatment (200 nM) showed increased levels of autophagy marker, LC3B-I[40], which is further increased by 3, 8, 1.5-fold with co-incubation of 5 nM CFZ at 1, 12 and 24 h, respectively, whereas, in DB76, a 13, 1.5, 3-fold increase was observed in LC3B-I at 1, 12 and 24 h, respectively. We also found that CFZ alone did not alter LC3B-I protein levels but induces oxidative stress response mediated cell death (**Fig. 1C**). Since accumulation of ROS is the early indicator of cellular apoptosis, we performed a flow cytometric analysis to evaluate the relative ROS levels upon drug treatment alone and in combination. A significant increase in ROS (by ~50%) is observed after 8 h of combination treatment with 200 nM CDDO-ME and 5 nM CFZ (**Fig. 1D**) as opposed to either CFZ or CDDO-ME separately in all four malignant astrocytoma patient derived cell lines. These results clearly indicate that LonP1 and CT-L inhibitors works synergistically than either drug alone in reducing cell viability by inducing reactive oxygen species mediated autophagy and apoptotic cell death in patient derived malignant astrocytoma.

3.2. Structure Activity Relationship Modeling for Developing CC4 Derivatives.

Our previous work with CC4 demonstrated that LonP1 inhibition could inhibit astrocytoma cell growth, adaptation to hypoxic conditions, and increase the anti-tumor efficacy of TMZ[22]. Coumarinic compounds have been found to exhibit high hepatotoxicity[41]. To decrease off-target toxicity and improve anti-tumor efficacy, we derived four novel LonP1 inhibitors from CC4 using structure-activity relationship (SAR) modeling. A library of small molecules (e.g., BT395, BT397, BT399, and BT317) was identified *in silico,* using customized computational protein structure modeling programs M4T, MMM, Mutate, and SAR with Autodock4, Surflex-Dock, ICM, PESD, and SFC (B. Das, unpublished data). Here, the CC4 ester group was modified to develop peptidomimetic compounds (amides and oxadiazoles) with increased water solubility. As a part of our rational design study, rings **A**, **B** and **C** were modified (**Fig. 2A**). Finally, the hydrophobic portion of rings **A** and **B** was replaced with quinolinolin-2 (1H)-1 to improve solubility (**Fig. 2B**; BT317). We also developed a library of additional CC4 derivatives; as shown in **Supplementary Fig. 2**. In Ring **A**, the benzyl group is prone to oxidation *in vivo* by oxidative cytochrome enzymes to form acidic chloride, which is associated with high toxicity. Therefore, chlorine was directly substituted at position 6 of the ring. The hydroxyl group on ring **C** was converted to a boronic ester group. The boronic acid and potassium salts of trifluoroborate and acid isosteres are known to increase cell permeability and reduce toxicity[42]. Furthermore, boronic acid and ester-based prodrugs were used as templates for ring **C** because boronic acid is selective for H_2O_2[33].

3.3. Novel CC4 Derivative, BT317, Exhibits On-Target dual Inhibition of LonP1 Protease and Proteasome Activity in enzymatic assays

Using our structure-activity relationship modeling approach, we derived BT317, BT395, BT397 and BT399 from CC4 and evaluated their relative LonP1 protease and proteasome inhibition profiles on purified protein. To evaluate the on-target inhibitory potency of these CC4 analog compounds, we assessed purified LonP1 protease activity inhibition using a FITC-casein substrate conversion in an enzymatic assay (**Fig. 3A and Supplementary Fig. 3A**). We purified the active LonP1 protein using the A/G Agarose magnetic resin and covalently immobilizing antibody by crosslinking with disuccinmidyl suberate, from a patient derived astrocytomas cell line overexpressing LonP1 and validated in SDS-PAGE gel and immunoblotting for LonP1 protein (**Fig. 3A)**. BT317 demonstrated purified LonP1 protease inhibition with an IC_{50}=31.2 μM, while BT397 exhibited similar inhibition at an IC_{50}

of 34.5 µM. The protease inhibitory activity in total mitochondrial lysate showed an IC_{50} of 48.8 µM and 51.3 µM with BT317 and BT397 respectively. The possible reason for the corresponding higher IC_{50} in total mitochondrial lysate compared with the purified LonP1 is because of the fact that same concentration of total mitochondrial lysate has less protease(s) quantity than purified LonP1 protease. The total mitochondrial lysate also contains fractions of other proteases that use the same casein substrate. The other inhibitors showed no inhibition of LonP1 protease activity (data not shown). We further found that subtracting ATP from the enzymatic reaction resulted in virtual elimination of the ATPase dependent LonP1 protease activity suggesting that LonP1 enzymatic activity is ATP dependent. Since some LonP1 inhibitors exhibit dual inhibition of LonP1 and proteasome[25], we next examined whether these CC4 analog compounds also can inhibit the 20S proteasome. For this assay, we prepared extracts from the established malignant glioma cell line, D-54 MG (**Fig. 3B**). At 10 µM, BT317 yielded a ~98 and 96% reduction in CT-L activity, a ~26% and 27% reduction in trypsin-like (T-L) activity, and a ~23% and ~30% reduction in caspase-like (C-L) activity at 1 and 4 h, respectively. The proteasomal activity of all three complexes returned to baseline at 8 h post-treatment. The BT395, BT397 and BT399 compounds moderately showed ~40, ~30 and ~50% inhibition of CT-L activity, whereas showed ~50, ~30 and ~50% reduction in T-L and ~50, ~30, ~40% reduction in C-L at 4h incubation, respectively (**Supplementary Fig. 3B-D**). 100nM Bortezomib (BTZ), which is a potent dual LonP1 and CT-L proteasome inhibitor approved for the treatment of multiple myeloma[44] was used here as a positive control.

From these results we found that out of all four CC4 analog compounds, BT317 demonstrated quicker kinetic inhibition of CT-L proteasome activity than BTZ (**Fig. 3B**).. The observed CT-L inhibition by BTZ demonstrates limited inhibition of ~20% in comparison to BT317, which showed ~90% inhibition early of 1 and 4 h incubation showing that BT317 is a more highly potent inhibitor of CT-L proteasome activity. Given the potent on-target LonP1 protease inhibition of BT317 and its accelerated CT-L proteasome inhibition, we selected BT317 for further evaluation as a dual LonP1/proteasome targeted therapy in our astrocytoma models.

The mitochondrial matrix protein aconitase (Aco2) and mitochondrial transcription factor A (TFAM) are known substrates of Lon proteolytic activity [31,45]. We examined the extent of Lon and two representative substrates, were modified after treatment with BT317. We treated the established glioma lines D-54 MG and U-87 MG with 10 µM BT317, which is well below the expected LonP1 protease inhibitory concentration, IC_{50} = 56.03 µM (**Fig. 3C**). Lon protein levels remained almost unchanged throughout in both the lines. The D-54 MG line responded with a pronounced Aco2 protein level increase of 2-fold at 1 h; which returned to the baseline levels by 8 and 24 hours. TFAM was still elevated by 3-fold at 24 h. In the U-87 line, BT317 resulted in the accumulation of Aco2 gradually to 3-fold and TFAM accumulated by 1.5-fold after 24 h. The LonP1 substrate accumulation exceeded what was expected way before LonP1 protease protein inhibition upon BT317 treatment (**Fig. 3C**). Together, these findings demonstrate that BT317 is a potent dual inhibitor of LonP1 protease and CT-L proteasome activity compared to any known dual inhibitor such as Bortezomib in established gliomas or patient derived astrocytoma.

3.4. BT317 induces autophagy, c-MET, FOXP1, p-AKT alone and shows synergy with standard of care Temozolomide through Reactive Oxygen Species dependent cell death in patient derived malignant astrocytoma

Current glioma research and clinical trials emphasize on the role of GSCs in tumor maintenance, resistance to therapies, and local invasion[46]. Patient derived astrocytoma lines used in this study are diverse for its genetic and epigenetic profiles like isocitrate IDH1/2 (mutant/wildtype), ATRX (retention/loss), and p53 (mutant/wildtype) **Supplemental Table 1**. The patient derived lines are enriched for tumor-initiating cancer stem cells because of passaging in serum-free media, suspension culture with referenced growth factors and have been shown to recapitulate the expression profile of the original patient sample[47]. Using the XTT assay, we determined the IC_{50} viability of established and patient derived GSC lines in response to 120 h of exposure to BT317 at graded doses (**Fig 4A and Supplementary Fig. S4A**). BT317 had increased toxicity towards the patient-derived GSC lines (i.e., 83MES, DB70, DB76, DB77, DB81; **Supplemental Table 1**) as compared to the established and differentiated astrocytoma lines, consistent with previous research which demonstrated that GSC are more sensitive to proteasome and LonP1 inhibition as compared with the more differentiated established lines[48]. The sensitivity of the DB70 line did not differ significantly from the DB81 line, derived from the same patient following recurrence. BT317 also showed less activity towards the CHLA-200 pediatric line (IC_{50}=85.88 µM). The normal cell lines, HPF242 and MCF10A, fibroblasts, and human astrocytes, also exhibited 4-8 fold higher viability following treatment with BT317 **Supplementary Fig. 4A**. Alongside we performed the viability study with TMZ alone to calculate the sensitivity of these patient derived glioblastoma line which came out to be an IC_{50} ranging anywhere between 17 to 22 µM (**Supplementary Fig. S4B**) and we decided to pick 10 µM concentration of TMZ which is less than the IC_{50} concentration to be used for the combination treatment in the further experiments. Furthermore, the cytotoxicity by BT317 synergized with 10 µM TMZ to decrease cell viability in the TMZ-resistant DB70, DB76, DB77 and 83MES GSC lines (recurrence following TMZ treatment) making them 5-6 fold more sensitive compared to the BT317 treatment alone (**Fig. 4A).** The two drugs in combination must need to be evaluated for the mechanism of interaction. The degree of interaction among the drugs either defines synergistic or anatagonistic interaction which is calculated using a reference model. The interactive analysis and visualization dose combination response data of BT317 and TMZ showed that the two drugs works synergistically, where a significantly low does of each drug in combination is more effective then individual effector drug doses **(Supplementary Fig. S4C)**. This kind of shows that we can use the BT317 in combination with standard of care TMZ at extremely low doses. Since early ROS accumulation is the readout of autophagic induction we did a time course (0, 1, 4, 8, 12 and 24h) treatment with 10uM BT317 and found that 8h is the time point where we see increase in the ROS relative mean intensity. With increasing time 12 and 24 h it goes down and plateaus eventually in both DB70 and 83MES lines **(Supplementary Fig. S4D)**. These results motivated us to focus on

the 8h time point for any further ROS study to perform combination treatment. Co-incubation of 10 µM BT317 with 10 µM TMZ in the DB70, DB76, DB77 and 83MES line resulted in a significant increase in ROS relative mean intensity by ~80, ~60, ~55 and ~60 %, respectively (**Fig. 4B**). BT317 alone did induce a significant increase in ROS relative mean intensity by ~30, ~40, ~35 and ~40 % at 8 h in the DB70, DB76, DB77 and 83MES line, respectively; however, no significant change in ROS relative mean intensities was observed upon TMZ treatment alone in any of the patient derived astrocytoma lines.

We next looked on the effect of BT317 inhibitor on the Aconitase and mitochondrial transcription factor A (TFAM) which are the are known substrates of Lon proteolytic activity. Protein profiles represents significant increase in Aco2 and TFAM at 24h with 10µM BT317 treatments in all patient derived malignant astrocytoma cell lines. DB70, DB76 and 83MES shows the multifold accumulation of substrate Aco2 at 24h where as DB77 show an early accumulation at 12h time point. TFAM accumulation follows the same trand among these cell lines (**Fig. 4C and Supplementary Fig. S4E**). We also evaluated the effect of BT317 on autophagy induction in these patient derived astrocytoma lines as a mechanism of cell death. We found that DB70 and DB76 are highly sensitive to autophagy induction with the LC3B levels shooting up as early as 1h of BT317 treatment. Whereas DB77 showed a delayed spike in LC3B-I levels by 7.62-fold that was reduced to 1.74-fold by 24 h.. The 83MES line did not show significant induction of autophagy even at 24h with BT317-.This muted autophagic response highlights the limited autophagy-induced cell death at 25uM BT317 in the DB77 line and the lack of autophagy-dependent cell death in the 83MES line, following co-incubation with 3mM 3-methyladenine (3-MA), an autophagy inhibitor. As expected DB70 and DB76, autophagy-dependent cell death was evident at lower concentrations of BT317 (**Fig. 4D and Supplementary Fig. S4F**). It was previously reported that TMZ targets more differentiated populations with an average IC_{50} of ~540 µM against similar glioma lines[49], whereas BT317 offers far greater efficacy against the harder to eradicate GSC populations (**Supplementary Table 1**) **Supplementary Fig. S4A**. Furthermore, these data highlight the potential use of BT317 in combination with TMZ as a treatment modality to target diverse cell populations with high LonP1 expression and potentially to reverse malignant astrocytoma treatment resistance independent of IDH, ATRX and p53 genetic profile.

3.5 LonP1 expression directy correlates with BT317 sensitivity in glioma cell lines

Our laboratory has previously demonstrated that cellular stress such as serum starvation, hypoxia and therapeutic stress such as radiation and chemotherapy (temozolomide) induces mitochondrial LonP1 expression. At the sametime, knocking down LonP1 using siRNA decreases cell viability and the use LonP1 inhibitors sensitize glioma cells to chemotherapy[22]. These previousy published findings suggest that glioma cells upregulate LonP1 protease as an adaptive response to overcome the effects of stress and acquire treatment resistance and aggressive malignant characteristics. Hence, the ability of inhibiting LonP1 activity by either pharmacological or genetic approaches presents interest as potential therapeutic for malignant glioma. However, the mechanisms of resistance to LonP1 inhibitors are not yet studied.

We genetically manipulated LonP1 expression in paired patient derived glioma lines and subjected them to BT317 treatment in a concentration dependent manner. Cell viability was measured after 5-days. We firstly ascertained that cells transduced for the gain (overexpression) and loss (knockdown) of LonP1 expression were validated through immunoblotting study (**Supplementary Fig. S5A)**. We found that vector control transfected cells i.e., +GFP with baseline LonP1 expression showed a moderate loss of cell viability with increasing concentrations of BT317 in all patients derived glioblastoma lines tested. In contrast, the cells overexpressing LonP1 losses the sensitivity to BT317 at even extremely high doses of 500 µM, making them ~15 fold less sensitive to control **(Fig. 5A and Supplementary Fig. S5B)**. The exact IC_{50} concentrations are mentioned in the individual graph. In contrast, BT317 treated cells expressing scramble control shRNA showed similar moderate decrease in viability under gradient BT317 concentration, whereas cells expressing LonP1 shRNA with the LonP1 knockdown were significantly sensitive to gradient drug concentration of BT317 making them ~4 fold more sensitive to control (Fig. 5A and Supplementary Fig.S5B).

Next, we decided to evaluate the apoptotic induction through ROS accumulation in our paired Lon overexpressing and knock-down patient derived astrocytoma lines. BT317 treatment alone significantly induces ROS accumulation in all malignant astrocytomas. In addition, our ROS relative mean intensities in all patient derived malignant astrocytomas lines showed a statistically significant increase in ROS accumulation upon combination treatment with TMZ, where TMZ alone has reltively low ROS induction at 8h incubation **(Fig. 5B and Supplementary Fig. S5C)**. The exact percentages are mentioned in the individual graph for our reference **(Fig. 5B and Supplementary Fig. S5C)**. We also found that LonP1 overexpression overall decrease the ROS accumulation in cells compared to their respective controls. The combination treatment of BT317 and TMZ is not been able to induce ROS even to the baseline control transfected(+GFP) cells. On the controray when we knocked down LonP1 cells become significantly more sensitive to the BT317 treatement alone and in combination. From here we can conclude that LonP1 directly provide tolerance to stress by decreasing the free radical accumulation in the cells.

To further validate the functional significance of Lon expression in glioma we performed a spheroid formation assay. Our results showed that LonP1 overexpression leads to significantly greater number of colony formation. In contrast, knocking down LonP1 led to a drastically low number of colonies in all patient derived astrocytoma lines (**Fig. 5C).** Spheroid formation assays further shows that LonP1 expression under gain (overexpression) and loss (knockdown) of function studies in patient derived glioblastoma cells directly regulates the sphere forming abilities of astrocytoma cells under isolation stress condition in of methylcellulose assay.

These findings demonstrate that the ability of cancer cells to upregulate LonP1 in response to nutrient stress[22] allows them to convert to a stress tolerant state and develop a more malignant behavior. LonP1 can be the biomarker of malignant attributes independent of genetic profile in these patient derived astrocytomas, explaining our previously published findings that Lon ex-

pression directly correlates with glioma patient survival [22]. Together, these results show that LonP1 is necessary and sufficient to drive BT317 mediated drug sensitivity and ROS mediated apoptosis in patient derived malignant astrocytomas. LonP1 overexpression rescued the inherent "drug sensitivity" of control cells, while LonP1 knockdown compromised the inherent "drug tolerance" of control cells, when evaluated using cell viability.

3.6. BT317 Exhibits Low Toxicity and its Activity is Localized to the Tumor and Combinatorial Treatment with TMZ Increases Survival

Previous development of proteasome inhibitors for the treatment of GBM was limited by either poor BBB penetrance (i.e., BTZ)[33] or by the presence of the central nervous system (i.e., MRZ= marizomib, confusion, ataxia)[50] or peripheral nervous system (BTZ, peripheral neuropathy)[51] toxicity. The development of these toxicities is directly related to the level of proteasome inhibition in the blood and in the normal brain[52].

Prior to evaluating efficacy, we established the maximum tolerated dose (MTD). Using a previously established methodology[38], we observed the clinical score following treatment (n=2) with iterative 50% dose escalation until we determined the MTD to be >180 mg/kg (data not shown). We repeated a continuous dose series over 10 days with 100 mg/kg of BT317 every other day or daily. There was no noticeable drop in weight or any observable clinical signs (**Fig. 6A**). Next, we administered 100 mg/kg BT317 and 25 mg/kg TMZ or 100 mg/kg BT317 and 50 mg/kg TMZ daily for 10 days. A temporary drop in weight and minor clinical signs were observed following the first 2 doses with 100 mg/kg BT317 and 50 mg/kg TMZ; however, the animal weight normalized by day 4 and no further clinical signs were observed. Since an ideal therapeutic candidate for malignant astrocytomas must have superior BBB penetrance, specifically target GSCs, synergize with the standard of care, TMZ, and demonstrate improved survival *in vivo,* we tested BT317 candidature for this as novel candidate. To assess BBB penetrance, 9x BALB/c mice received a single intraperitoneal (i.p.) injection of BT317 (3 mg/kg). The animals were euthanized 30, 60, and 120 min post-BT317 injection (n=3 per endpoint). Brain and plasma samples were collected, and BT317 (ng/mL) levels were quantified using mass spectrometry (**Fig. S6A**). BT317 levels reached ~390 ng/mL in the brain at 30 min and decreased to ~55 ng/mL at 120 min post-injection. At all measured endpoints, levels in the brain were significantly higher than those in the plasma.To evaluate the target specific activity of BT317, we performed an intracranial implantation of the DB70 line and after 15 days of implant, administered a single dose of 100 mg/kg of BT317 to the mice prior to analyzing proteasome activity in the blood, healthy brain, and intracranial tumor mass (**Fig. 6B**). The animals were euthanized 1 and 4 h post-injection (n=6 per endpoint). BT317 showed ~70% and 60% inhibition of CT-L and C-L activity in the tumor, respectively, compared with ~50% and 25% for MRZ at 4 h. Only MRZ showed CT-L inhibition in the normal healthy brain with a ~40% reduction at 1-4 h. Furthermore, MRZ also inhibited CT-L, T-L, and C-L in the blood by ~90%, 35-45%, and 30%, respectively. BT317 did not inhibit proteasome activity in the blood. Both BT317 and MRZ showed accumulation of Aco2 in the tumor at 4 h with ~60-70% increase on average (**Fig. 6B**).

Next, we assessed the efficacy in an orthotopic xenograft model using the GSC patient derived, DB70 and DB76 lines. Rag1 KO mice were intracranially implanted with DB70 or DB76 (1000 cells/mouse), dissociated from a fresh in vitro, organoid model[39] (**Fig. 6C**). A total of 5 doses were administered at 100 mg/kg BT317 ± 50 mg/kg TMZ daily, starting 10 days after intracranial xenograft implantation and continuing for a total of 5 days. Our results showed that BT317 alone significantly improved the median survival by 1 ($p<0.05$) and 3 days ($p<0.05$) in the DB70 and DB76 xenografts, respectively. The combination of BT317 and TMZ significantly improved overall survival ($p<0.01$); however, median survival for the combinatorial cohorts could not be determined by the end of the experiment. We also found that earlier dosing regimen starting on day 5 for a total 5 doses of 100 mg/kg BT317 every other day significantly increased median survival from 25 to 33 days in the DB70 PDX model (10,000 cells/mouse, **Supplementary Fig. 6C**). The 83MES PDX model also showed a modest increase in median overall survival from 17.5 to 19 days; however, this required an escalated dosage of 150 mg/kg BT317 (10,000 cells/mouse, **Supplementary Fig. 6D**). Together, here we found that BT317 is well tolerated at exceptionally high dose, with good BBB permeability, on target tumor accumulation, showing little to no off-target proteasome inhibition. Further BT317 together with standard of care TMZ showed synergistic effect with prolonged median survival in orthotopic model. These results clearly showed that BT317 could be an ideal therapeutic candidate for LonP1 specific malignant astrocytomas subtype both alone or in combination with standard of care TMZ.

4. Discussion and Conclusion

Malignant astrocytomas are still waiting for potent therapeutics to control the frequent relapse and therapy resistance. Previously, we demonstrated that the LonP1 inhibitor, CC4, was effective against established glioma lines and the proteasome inhibition with marizomib is effective in *in vitro* and *in vivo* glioma models, though its clinical use is limited by significant CNS toxicity[53]. Here we have reported the designing of the novel dual LonP1 and CT-L proteasome inhibitor, BT317, which has specific activity and limited toxicity with better blood brain barrier permeability *in vivo,* on-target effects compared with currently available proteasome inhibitors.

For our rational design and SAR modeling, we used customized computational protein structure modeling programs, as well as standard programs, to identify the lead compounds that could be derived from CC4 to improve solubility and BBB permeability and reduce toxicity. For compound design, we used the standard Lipinski rule of 5 with the following considerations: (1) pharmacological or biological activity (i.e., more sp3 carbon atoms), (2) ease of synthesis, and (3) moderate compound complexity to minimize toxicity and off-target effects[54].

Our lead molecule, BT317, exhibited dual inhibition of LonP1 protease activity and CT-L proteasomal activity, on-target LonP1 inhibition, BBB permeability, low animal toxicity, and prolonged survival with and without the standard-of-care (TMZ) in two patient-derived GSC intracranial xenograft models. BT317 accumulated at higher levels in the brain than in the plasma at 30 min post-administration. Its potent dual inhibitory activity can be compared with that of BTZ, a potent proteasome inhibitor that also inhibits LonP1 protease activity. However, BTZ has limited penetrance into the brain, and a phase II clinical trial of BTZ and bevacizumab in recurrent GBM was hindered due to dose-limiting sensory neuropathy associated with BTZ[55]. Another CT-L proteasome inhibitor tested for GBM was ritonavir. Nonetheless, ritonavir failed to demonstrate efficacy due to the development of resistance, *in vivo*[56]. Marizomib has also shown improved survival in orthotopic GBM models; however, it has exhibited underlying issues with significant CNS toxicity (confusion, ataxia, fatigue)[57] in phase 2 studies and did not improve survival in a phase 3 randomized clinical trial[50]. This toxicity is represented by the high rate of marizomib-treated patients that have neurologic (67%) and psychiatric (52%) adverse events[53]. Additionally, the high MTD and specific tumor activity of BT317 further demonstrates its potential as a less toxic dual LonP1 and proteasomal inhibitor for GBM treatment.

GBM is characterized by mitochondrial dysfunction, including metabolic shifts towards aerobic glycolysis, elevated ROS generation, and sensitivity to metabolic stress[22]. Aconitase participates in the tricarboxylic acid cycle (TCA) by converting citrate to isocitrate; however, its involvement in malignant astrocytoma metabolism is unclear. Recent studies have shown that Aco2 levels are decreased in breast cancer cell lines and patient-derived tumor biopsies, and Aco2 overexpression impairs breast cancer cell proliferation and mitigates the Warburg effect by redirecting pyruvate to the mitochondria[58]. In addition to its role in the TCA cycle, aconitase also promotes mtDNA stability by interacting with nucleoids (protein-mtDNA complexes)[59]. Lon protease degrades aconitase and prevents aconitase accumulation[45]. Our findings revealed pronounced Aco2 accumulation in stable GBM lines and patient derived GSCs following BT317 exposure. Notably, BT317 induced Aco2 accumulation at 10 µM despite the IC_{50}=31 µM for LonP1 protease inhibition. This accumulation was more pronounced than that induced by 100 nM BTZ, with previously reported LonP1 protease inhibition (IC_{50}=60 nM)[32]. BT317 also increased Aco2 levels in an intracranial xenograft model. Further investigation of the role of Aco2 in malignant astrocytoma metabolism is warranted.

An important finding of our study is that the combination of BT317 and TMZ is more effective than BT317 or TMZ alone in in all four patient derived astrocytoma lines independent of their genetic profile like IDH1/2 mutant/wildtype, ATRX (retention/loss), and p53 (mutant/wildtype). We previously found that LonP1 is the biomarker for aggressive and malignant subtypes of astrocytomas [22]. LonP1 is directly involved in imparting tolerance under isolation stress in astrocytomas as observed in spheroid formation assay which is an established mechanism of aggressive recurrence and drug resistance. The normal human fibroblast cell lines, HPF242 and MCF-10A, were less sensitive to BT317 treatment. TMZ has been found to induce mTOR signaling (e.g., pAKT)[66,67] and also subsequently block autophagy[67] in the 12-60 h range. This inhibition of autophagy likely explains the strong synergy between TMZ and BT317, as BT317 clearly strongly induces autophagy and we clearly proved that blocking autophagy with 3-MA was found to induce cell death. This study further validated that LonP1 is required to drive resistance (gain of function study) and sufficient to drive sensitivity (loss of function study) BT317 mediated drug sensitivity. LonP1 targeting by BT317 regulates cellular ROS levels inducing apoptosis in patient derived malignant astrocytomas. BT317 in combination with standard of care therapy TMZ significantly sensitizes BT317 resistant LonP1 overexpressing cells, while LonP1 knockdown compromised the inherent "drug tolerance" of control cells, when evaluated using cell viability and sphere formation assay.

Another aspect of LonP1 targeting using combination of TMZ and BT317 that might be interesting to explore (but not covered in this study) is its role in modulating unfolded protein response (UPR). The endoplasmic reticulum (ER) and mitochondrial unfolded protein response pathways (UPRER and UPRmt, respectively) have been postulated to impart an advantage to cancer cells, supporting cell survival, proliferation, and evasion of immune surveillance, and drug resistance [68-70], by mitigating hostile conditions within the tumor microenvironment such as nutrient and oxygen deprivation, oxidative stress, and high metabolic demand. Additionally, the maximum tolerated dose was exceptionally high, with little to no off-target proteasome inhibition. Targeting the GSC population is critical for overcoming glioma treatment resistance. Proteasome activity also plays a key role in cancer treatment resistance[27,28]. Interestingly, gliomas have elevated CT-L proteasome activity and, generally, an increase in this activity serves as a compensatory response to prooxidative treatment[71]. Additional studies are vital to further explore the role of LonP1 and CT-L proteasome activity in malignant glioma metabolism and whether dual inhibition could be useful for treating recurrent malignant astrocytoma based on patient-specific genetic determinants. Future work will also seek to understand the best route of administration, while also creating BT317 analogs that incorporate nanoparticles and other moieties to optimize on-site and on-target activity to further the development of new therapeutic options for malignant astrocytoma patients.

Figure Legend

Figure 1. Dual LonP1 and Chymotrypsin-like Proteasome Inhibition has Greater Synergy in Malignant Astrocytoma showing Enhanced Autophagy and ROS Production

A. DB70, DB76, DB77and 83MES cells were incubated with the indicated concentrations of CDDO-ME with or without indicated concentrations of CFZ, for 48 h. The cell viability was measured using XTT reagent at the end of the incubation period. Error bars indicate the standard deviations of three biological replicates. n = 3 technical replicates from 3 biological replicates for each group.

584 **B**. A synergy test between CDDO-ME and CFZ combination was performed with XTT data using online tool SynergyFinder - Doc-
585 umentation (fimm.fi).
586 **C.** Autophagy maker LC3B protein expression levels were measured after indicated time treatment with 5nM CFZ and/or 200nM
587 CDDO-ME.
588 **D.** ROS levels were assessed following treatment with 5nM CFZ and/or 200nM CDDO-ME at 8 h timepoints in DB70 DB76, DB77
589 and MES83. Statistical significance was determined by t-test. * *P* <0.05, ***P* <0.01, ****P* <0.001; ns, not significant.

590 **Figure 2. LonP1 small molecule inhibitor BT317 was derived from CC4.** (**A**) BT317 is an analog of CC4. (**B**) Synthesis steps of
591 BT317.

592 **Figure 3. BT317 acts as a dual inhibitor of LonP1 and chymotrypsin-like CT-L proteasome activity**.
593 **A.** LonP1 Protease was purified through antibody crosslinking and Immunoprecipitated from mitochondrial lysate of patient-
594 derived DB70 cells, verified with on tris-glycine gel using Coomassie staining (Left) and immunoblotted with LonP1 antibody
595 (middle). The gradient concentration of BT317 was added to purified LonP1 protease lysate or equivalent total mitochondrial
596 lysate and incubated for 1h at 37°C. At the end of incubation, fluorescent FITC-Casein substrate was added to measure the ef-
597 fect of BT317 on enzyme activity (right). BT317 was assessed for inhibition of protease activity with an IC_{50} established at 31.2
598 µM with purified lonP1 protease whereas total mitochondrial lysate showed the inhibition of protease activity with IC_{50} 48.8
599 µM. Subtracting ATP from the reaction deactivates the overall enzyme activity. The calculations are based on results from three
600 independent experiments.
601 **B.** 10µM BT317 were evaluated for proteasome inhibition at 1, 4, 6, 8 h. 100nM BTZ was used as a positive control on pro-
602 teasome inhibition.BTZ = Bortezomib; CT-L= Chymotrypsin-like activity; T-L = Trypsin-like activity; C-L = Caspase-like activity.
603 Statistical significance was determined by t-test. * P <0.05, **P <0.01, ***P <0.001; n.s., not significant.
604 **C.** The U-251 and U-87 MG established glioma lines were treated with 20µM BT317 and demonstrated increased Aco2 and
605 TFAM levels. Data are presented as mean ± SEM of at least 3 replicates. Statistical significance was determined by t-test. * *P*
606 <0.05, ***P* <0.01, ****P* <0.001; n.s., not significant.

607 **Figure 4. BT317 drives cell death in malignant astrocytomas and TMZ works synergistically.**
608 **A**. DB70, BD76, DB77 and 83MES astrocytoma were incubated with the indicated concentrations of BT317 with or without
609 standard of care, TMZ (10 µM), for 120 h. The cell viability was measured at the end of the incubation period. Error bars indicate
610 the standard deviations of three biological replicates. n = 3 technical replicates from 3 biological replicates for each group.
611 **B.** Patient derived malignant astrocytoma cells were incubated with 10 µM BT317 with or without standard of care, TMZ (10
612 µM), for 8h. ROS was detected at the end of incubation using deep red oxidative stress reagent through flow cytometry. Rela-
613 tive mean intensities were calculated for each group. Error bars indicate the standard deviations of three biological replicates. n
614 = 3 technical replicates from 3 biological replicates for each group. Statistical significance was determined by 2way ANOVA. * P
615 <0.05, **P <0.01, ***P <0.001; n.s., not significant.
616 **C**. Protein expression levels of Lon substrate Aco2 and TFAM and autophagy marker LC3Band pAKT were evaluated at 10 µM
617 BT317 for 1-24 h.
618 D. The malignant astrocytoma lines DB70 and 83MES were analyzed for cell death following treatment with a titer of BT317 and
619 co-incubation with 3mM 3-MA for 5 days. Statistical significance was determined by t-test. * P <0.05, **P <0.01, ***P <0.001;
620 n.s., not significant.

621 **Figure 5. LonP1 is necessary and sufficient to drive sensitivity to BT317 in LonP1 overexpressing and knockdown genetic mod-**
622 **el.**
623 **A.** DB70 and DB77 cells with and without LonP1 expression (+LonP1 and +GFP, respectively) and corresponding cells with and
624 without LonP1 knockdown (shLonP1 and shSCR, respectively) were incubated with the indicated concentrations of BT317 for
625 120 h. The cell viability was measured at the end of the incubation period. Error bars indicate the standard deviations of three
626 biological replicates. n = 3 technical replicates from 3 biological replicates for each group.
627 **B.** DB70and DB77 cells with and without LonP1 expression (+LonP1 and +GFP, respectively) and corresponding cells with and
628 without LonP1 knockdown (shLonP1 and shSCR, respectively) were incubated with 10 µM BT317 with or without standard of
629 care, TMZ (10 µM), for 8h. ROS was detected at the end of incubation using deep red oxidative stress reagent through flow
630 cytometry. Relative mean intensities were calculated for each group. Error bars indicate the standard deviations of three biolog-
631 ical replicates. n = 3 technical replicates from 3 biological replicates for each group. Statistical significance was determined by
632 2way ANOVA. * P <0.05, **P <0.01, ***P <0.001; n.s., not significant.

C. Sphere formation assay: Patient derived glioblastoma cells DB70 and DB77 with LonP1 overexpression (+LonP1), LonP1 knockdown (+shLonP1), or no modification (+GFP) or scrambled control (+shSCR) were incubated with methylcellulose for 14 days. The panel shows experimental design and graphical representation of number of colonies and the representative images. % area of colonies was measured. ***P<0.005, compared to +GFP or +shSCR, using ANOVA. Error bars indicate the standard deviations of three biological replicates. n = 2 technical replicates from 3 biological replicates for each group.

Figure 6. The combination of BT317 and TMZ shows minimal toxicity in NSG mice and Treatment Significantly Improves Survival.

A. Maximum tolerated dose of BT317 was determined alone and in combination with the standard of care, TMZ. BT317 was administered intraperitonially (i.p.)) at 100mg/kg every other or daily for 10 total days and 100mg/kg of BT317 ± 25 or 50 mg/kg TMZ were administered daily for total of 10 days. Percent weight change and clinical score were monitored every day.

B. In vivo site-specific vital activity of BT317 was determined using tumor xenograft. Patient derived DB70 cells were intracranial implanted for 15 days, single dose of BT317 (100mg/kg), Marizomib (50µg/kg) or DMSO (w/v) were injected i.p. 1h and 4 h prior to euthanasia. Proteasome activities and Aco2 protein levels were measured in the blood, healthy brain, and intracranial tumor mass. Error bars indicate the standard deviations of six biological replicates (n=6). Statistical significance was determined by 2way ANOVA. * *P* <0.05, ***P* <0.01, ****P* <0.001; n.s., not significant.

C. Rag1 KO mice were intracranially implanted with DB70 or DB76 (1000 cells/mouse), dissociated from a novel in vitro, organoid model. 10 days after intracranial implantation, 100 mg/kg BT317 ± 100 mg/kg TMZ was injected i.p. daily for 5 days. The median survival methodology was applied to assess any survival advantage in the intracranial xenograft model. Average weights of animals were tracked from post-implantation for DB70 and DB76. Significance was measured n=3 per endpoint).; *p<0.05, **p<0.01, ***p<0.001 ns=not significant. (BT317, n=6; MRZ, n=6, DMSO n=4 per endpoint).

Supplementary Materials: The Supplementary figures are provided as a separate .pptx file.

Funding: This work was supported by the National Institute of Neurologic Diseases and Stroke Award (NINDS/NIH) [NS109423] to DAB and BD. This work was also supported by the NINDS/NIH Award [NS111303], the National Center for Advancing Translational Sciences (NCATS/NIH) Award [UL1 TR001414], the UCI American Cancer Society Institutional Grant [ACS/IRG – 98-279- 07], the Ruth L. Kirschstein National Research Service T32 Award [2T32CA009054-41 (MPI)] and the UCI Cancer Center Award [P30CA062203] from the National Cancer Institute to DAB. *The content is solely the responsibility of the authors and does not necessarily represent the official views of the National Institutes of Health.*

Institutional Review Board Statement: The study was conducted in accordance with the Declaration of Helsinki and approved by the Institutional Review Board (or Ethics Committee) of University of California Irvine (protocol code UCI IRB HS#2012-8912, CMU Reliance #78 and date of approval is 05/31/2019)." for studies involving humans. And the animal study protocol was approved by the Institutional Review Board (or Ethics Committee) of University of California Irvine (protocol code AUP-23-024, subject to 3-year renewal, replaces AUP-20-022 and approval period for 03/21/2023-03/21/2026)." for studies involving animals.

Informed Consent Statement: "Informed consent was obtained from all subjects involved in the study.

Conflicts of Interest: The authors have no conflicts of interest to disclose.

Authorship Statement: Conception and design of this work: DAB, BD, CD, SJ KD, and NL. Inhibitor synthesis and design: BD and NKD. Brain mass spectrometry measurements: Cyprotex and Biotechnology Innovation and Optimization Center. Data collection, analysis,F and interpretation: CD, SJ. All the authors critically reviewed and approved the final manuscript.

Data Access Statement: Research data supporting this publication are as presented in the manuscript.

References

1. Ohgaki, H., *et al.* Genetic Pathways to Glioblastoma: A Population-Based Study. *Cancer research* **64**, 6892-6899 (2004).
2. Sathornsumetee, S., Rich, J.N. & Reardon, D.A. Diagnosis and Treatment of High-Grade Astrocytoma. *Neurologic Clinics* **25**, 1111-1139 (2007).
3. Stupp, R., *et al.* Radiotherapy plus concomitant and adjuvant temozolomide for glioblastoma. *N Engl J Med* **352**, 987-996 (2005).
4. Rominiyi, O., *et al.* Tumour treating fields therapy for glioblastoma: current advances and future directions. *British Journal of Cancer* **124**, 697-709 (2021).
5. Fisher, J.P. & Adamson, D.C. Current FDA-Approved Therapies for High-Grade Malignant Gliomas. *Biomedicines* **9**(2021).

6. Hegi, M.E., *et al.* MGMT gene silencing and benefit from temozolomide in glioblastoma. *N Engl J Med* **352**, 997-1003 (2005).
7. Ohgaki, H. & Kleihues, P. The definition of primary and secondary glioblastoma. *Clin Cancer Res* **19**, 764-772 (2013).
8. Louis, D.N., *et al.* The 2021 WHO Classification of Tumors of the Central Nervous System: a summary. *Neuro-Oncology* **23**, 1231-1251 (2021).
9. Yan, H., *et al.* IDH1 and IDH2 mutations in gliomas. *N Engl J Med* **360**, 765-773 (2009).
10. Golub, D., *et al.* Mutant Isocitrate Dehydrogenase Inhibitors as Targeted Cancer Therapeutics. *Front Oncol* **9**, 417 (2019).
11. Liu, Y., *et al.* Targeting IDH1-Mutated Malignancies with NRF2 Blockade. *J Natl Cancer Inst* **111**, 1033-1041 (2019).
12. Li, Z., *et al.* Hypoxia-inducible factors regulate tumorigenic capacity of glioma stem cells. *Cancer Cell* **15**, 501-513 (2009).
13. Gordan, J.D., Thompson, C.B. & Simon, M.C. HIF and c-Myc: Sibling Rivals for Control of Cancer Cell Metabolism and Proliferation. *Cancer Cell* **12**, 108-113 (2007).
14. Forsythe, J.A., *et al.* Activation of vascular endothelial growth factor gene transcription by hypoxia-inducible factor 1. *Molecular and Cellular Biology* **16**, 4604-4613 (1996).
15. Kaur, B., *et al.* Hypoxia and the hypoxia-inducible-factor pathway in glioma growth and angiogenesis. *Neuro-oncology* **7**, 134-153 (2005).
16. Yang, L., Lin, C., Wang, L., Guo, H. & Wang, X. Hypoxia and hypoxia-inducible factors in glioblastoma multiforme progression and therapeutic implications. *Experimental Cell Research* **318**, 2417-2426 (2012).
17. Fukuda, R., *et al.* HIF-1 regulates cytochrome oxidase subunits to optimize efficiency of respiration in hypoxic cells. *Cell* **129**, 111-122 (2007).
18. Rep, M., *et al.* Promotion of mitochondrial membrane complex assembly by a proteolytically inactive yeast Lon. *Science (New York, N.Y.)* **274**, 103-106 (1996).
19. Liu, T., *et al.* DNA and RNA binding by the mitochondrial lon protease is regulated by nucleotide and protein substrate. *The Journal of biological chemistry* **279**, 13902-13910 (2004).
20. Quiros, P.M., *et al.* ATP-dependent Lon protease controls tumor bioenergetics by reprogramming mitochondrial activity. *Cell Rep* **8**, 542-556 (2014).
21. Cheng, C.W., *et al.* Overexpression of Lon contributes to survival and aggressive phenotype of cancer cells through mitochondrial complex I-mediated generation of reactive oxygen species. *Cell Death Dis* **4**, e681 (2013).
22. Di, K., Lomeli, N., Wood, S.D., Vanderwal, C.D. & Bota, D.A. Mitochondrial Lon is over-expressed in high-grade gliomas, and mediates hypoxic adaptation: potential role of Lon as a therapeutic target in glioma. *Oncotarget* **7**, 77457-77467 (2016).
23. Erina Vlashia, C.L., Laurent Vergnesb, Tomoo Matsutanic, Kenta Masuic, Maria Pouloua, Ruxandra Popescua, Lorenza Della Donnaa, Patrick Eversa, Carmen Dekmeziana, Karen Reueb,d, Heather Christofke,f,Paul S. Mischelc,f, and Frank Pajonk. Metabolic state of glioma stem cells and non tumorigenic cells. *PNAS*, 16062-16067 (2011).
24. Stoll, M.S.a.E.A. Metabolic Reprogramming in Glioma. *Front Cell Dev Biol*, 5:43 (2017).
25. Bayot, A., *et al.* Towards the control of intracellular protein turnover: Mitochondrial Lon protease inhibitors versus proteasome inhibitors. *Biochimie* **90**, 260-269 (2008).
26. Stahlberg, H., *et al.* Mitochondrial Lon of Saccharomyces cerevisiae is a ring-shaped protease with seven flexible subunits. *Proceedings of the National Academy of Sciences* **96**, 6787-6790 (1999).
27. Adams, J. The proteasome: structure, function, and role in the cell. *Cancer Treat Rev* **29 Suppl 1**, 3-9 (2003).
28. Patel, N.M., *et al.* Paclitaxel sensitivity of breast cancer cells with constitutively active NF-kappaB is enhanced by IkappaBalpha super-repressor and parthenolide. *Oncogene* **19**, 4159-4169 (2000).
29. Maneix, L., *et al.* The Mitochondrial Protease LonP1 Promotes Proteasome Inhibitor Resistance in Multiple Myeloma. *Cancers (Basel)* **13**(2021).
30. Lee, J., *et al.* Inhibition of mitochondrial LonP1 protease by allosteric blockade of ATP binding and hydrolysis via CDDO and its derivatives. *The Journal of biological chemistry* **298**, 101719 (2022).

31. Gibellini, L., *et al.* Inhibition of Lon protease by triterpenoids alters mitochondria and is associated to cell death in human cancer cells. *Oncotarget* **6**, 25466-25483 (2015).
32. Csizmadia, V., *et al.* Proteasome inhibitors bortezomib and carfilzomib used for the treatment of multiple myeloma do not inhibit the serine protease HtrA2/Omi. *Toxicol Res (Camb)* **5**, 1619-1628 (2016).
33. Takeshima, K., Mizuno, K., Nakahashi, H., Aoki, H. & Kanekiyo, Y. Ratiometric Sensing of Hydrogen Peroxide Utilizing Conformational Change in Fluorescent Boronic Acid Polymers. *Journal of Analytical Methods in Chemistry* **2017**, 7829438 (2017).
34. Huehnchen, P., *et al.* Bortezomib at therapeutic doses poorly passes the blood–brain barrier and does not impair cognition. *Brain Communications* **2**(2020).
35. Tang, J.H., *et al.* Bortezomib inhibits growth and sensitizes glioma to temozolomide (TMZ) via down-regulating the FOXM1-Survivin axis. *Cancer Commun (Lond)* **39**, 81 (2019).
36. Seidel, S., Garvalov, B.K. & Acker, T. Isolation and Culture of Primary Glioblastoma Cells from Human Tumor Specimens. in *Stem Cell Protocols* (ed. Rich, I.N.) 263-275 (Springer New York, New York, NY, 2015).
37. Van der Borght, K., *et al.* BIGL: Biochemically Intuitive Generalized Loewe null model for prediction of the expected combined effect compatible with partial agonism and antagonism. *Sci Rep* **7**, 17935 (2017).
38. Aston, W.J., *et al.* A systematic investigation of the maximum tolerated dose of cytotoxic chemotherapy with and without supportive care in mice. *BMC cancer* **17**, 684-684 (2017).
39. Hubert, C.G., *et al.* A Three-Dimensional Organoid Culture System Derived from Human Glioblastomas Recapitulates the Hypoxic Gradients and Cancer Stem Cell Heterogeneity of Tumors Found In Vivo. *Cancer research* **76**, 2465-2477 (2016).
40. Mizushima, N. & Yoshimori, T. How to interpret LC3 immunoblotting. *Autophagy* **3**, 542-545 (2007).
41. Vassallo, J.D., Hicks, S.M., Daston, G.P. & Lehman-McKeeman, L.D. Metabolic Detoxification Determines Species Differences in Coumarin-Induced Hepatotoxicity. *Toxicological Sciences* **80**, 249-257 (2004).
42. Lassalas, P., *et al.* Structure Property Relationships of Carboxylic Acid Isosteres. *Journal of medicinal chemistry* **59**, 3183-3203 (2016).
43. Halasi, M., *et al.* ROS inhibitor N-acetyl-L-cysteine antagonizes the activity of proteasome inhibitors. *Biochemical Journal* **454**, 201-208 (2013).
44. Manton, C.A., *et al.* Induction of cell death by the novel proteasome inhibitor marizomib in glioblastoma in vitro and in vivo. *Scientific Reports* **6**, 18953 (2016).
45. Bota, D.A. & Davies, K.J. Lon protease preferentially degrades oxidized mitochondrial aconitase by an ATP-stimulated mechanism. *Nature cell biology* **4**, 674-680 (2002).
46. Chen, J., *et al.* A restricted cell population propagates glioblastoma growth after chemotherapy. *Nature* **488**, 522-526 (2012).
47. Vik-Mo, E.O., *et al.* Brain tumor stem cells maintain overall phenotype and tumorigenicity after in vitro culturing in serum-free conditions. *Neuro Oncol* **12**, 1220-1230 (2010).
48. Gong, X., Schwartz, P.H., Linskey, M.E. & Bota, D.A. Neural stem/progenitors and glioma stem-like cells have differential sensitivity to chemotherapy. *Neurology* **76**, 1126-1134 (2011).
49. Ferretti, M., *et al.* M2 receptor activation inhibits cell cycle progression and survival in human glioblastoma cells. *Journal of cellular and molecular medicine* **17**(2013).
50. Di, K., *et al.* Marizomib activity as a single agent in malignant gliomas: ability to cross the blood-brain barrier. *Neuro-oncology* **18**, 840-848 (2016).
51. Rutkowski, S., *et al.* Treatment of early childhood medulloblastoma by postoperative chemotherapy and deferred radiotherapy. *Neuro-Oncology* **11**, 201-210 (2009).
52. Velasco, R., Alberti, P., Bruna, J., Psimaras, D. & Argyriou, A.A. Bortezomib and other proteasome inhibitors—induced peripheral neurotoxicity: From pathogenesis to treatment. *Journal of the Peripheral Nervous System* **24**, S52-S62 (2019).
53. Roth, P., *et al.* EORTC 1709/CCTG CE.8: A phase III trial of marizomib in combination with temozolomide-based radiochemotherapy versus temozolomide-based radiochemotherapy alone in patients with newly diagnosed glioblastoma. in *ASCO Annual Meeting*, Vol. Central Nervous System Tumors (2021).
54. Lovering, F., Bikker, J. & Humblet, C. Escape from flatland: increasing saturation as an approach to improving clinical success. *Journal of medicinal chemistry* **52**, 6752-6756 (2009).

786 55. Bota, D.A., *et al.* Phase II clinical trial of bortezomib and bevacizumab combination in recurrent
787 glioblastoma. *Journal of Clinical Oncology* **29**, 2056-2056 (2011).
788 56. Laurent, N., *et al.* Effects of the proteasome inhibitor ritonavir on glioma growth in vitro and in vivo. *Mol*
789 *Cancer Ther* **3**, 129-136 (2004).
790 57. Bota, D.A., *et al.* Marizomib alone or in combination with bevacizumab in patients with recurrent
791 glioblastoma: Phase I/II clinical trial data. *Neurooncol Adv* **3**, vdab142-vdab142 (2021).
792 58. Ciccarone, F., *et al.* Aconitase 2 inhibits the proliferation of MCF-7 cells promoting mitochondrial oxidative
793 metabolism and ROS/FoxO1-mediated autophagic response. *British Journal of Cancer* **122**, 182-193 (2020).
794 59. Farooq, M.A., Pracheil, T.M., Dong, Z., Xiao, F. & Liu, Z. Mitochondrial DNA Instability in Cells Lacking
795 Aconitase Correlates with Iron Citrate Toxicity. *Oxidative Medicine and Cellular Longevity* **2013**, 493536
796 (2013).
797 60. Li, L.C., Zhang, M., Feng, Y.K. & Wang, X.J. IDH1-R132H Suppresses Glioblastoma Malignancy through FAT1-
798 ROS-HIF-1α Signaling. *Neurol India* **68**, 1050-1058 (2020).
799 61. Williams, S.C., *et al.* R132H-mutation of isocitrate dehydrogenase-1 is not sufficient for HIF-1α upregulation
800 in adult glioma. *Acta Neuropathol* **121**, 279-281 (2011).
801 62. Yao, J., *et al.* Metabolic characterization of human IDH mutant and wild type gliomas using simultaneous pH-
802 and oxygen-sensitive molecular MRI. *Neuro-Oncology* **21**, 1184-1196 (2019).
803 63. Xu, W., *et al.* Oncometabolite 2-Hydroxyglutarate Is a Competitive Inhibitor of α-Ketoglutarate-Dependent
804 Dioxygenases. *Cancer Cell* **19**, 17-30 (2011).
805 64. Li, K., *et al.* IDH1 R132H mutation regulates glioma chemosensitivity through Nrf2 pathway. *Oncotarget* **8**,
806 28865-28879 (2017).
807 65. Dao Trong, P., *et al.* Identification of a Prognostic Hypoxia-Associated Gene Set in IDH-Mutant Glioma. *Int J*
808 *Mol Sci* **19**(2018).
809 66. Murphy, S.F., *et al.* Connexin 43 Inhibition Sensitizes Chemoresistant Glioblastoma Cells to Temozolomide.
810 *Cancer research* **76**, 139-149 (2016).
811 67. Yu, Z., *et al.* Metformin and temozolomide act synergistically to inhibit growth of glioma cells and glioma
812 stem cells in vitro and in vivo. *Oncotarget* **6**, 32930-32943 (2015).
813 68. C.M., M.E.S.R.A.T.-T.J.C.Y.I.P.P.K.K.d.M.P.A.M.J.Z.S.T. The unfolded protein response mediator PERK governs
814 myeloid cell-driven immunosupression in tumor through inhibition of STING signaling. *Immunity* **52**, 668-682
815 (2020).
816 69. L.H., C.-R.J.R.B.S.E.G. Tumorigenic and immunosuppressive effects of endoplasmic reticu-lum stress in
817 cancer. *Cell* **168**, 692-706 (2017).
818 70. C.M., D.P.H. Mitochondrial dysfunction in cancer: Potential roles of ATF5 and the mitochondrial UPR *Semin.*
819 *Cancer Biol.* **47**, 43-49 (2017).
820 71. Kretz-Remy, C. & Arrigo, A.-P. Modulation of the chymotrypsin-like activity of the 20S proteasome by
821 intracellular redox status: effects of glutathione peroxidase-1 overexpression and antioxidant drugs. *Biol*
822 *Chem* **384**, 589-595 (2003).

823

824

825

826

827

828

829

830

831

832

833

834

835

836

837

838

839

840

841

842 **Table 1. Lines for patient-derived samples and established included in this study.**

843

Patient-derived GSC Lines						
Line	Classification	Grade	IDH1	p53	ATRX	IC50 conc of BT317
DB70	Astrocytoma	3	Mut	Lost	Lost	41.30
DB76	Astrocytoma	4	Mut	Lost	Lost	53.5
DB77	Astrocytoma	4	WT	WT	WT	72.3
83MES	Glioblastoma	4	WT	N/A	N/A	63.7
DB81	Astrocytoma	4	Mut	Lost	Lost	45.7
U-251 MG	Glioblastoma		WT	Mut	WT	82.06
D-54 MG	Glioblastoma		WT	Mut	WT	63.29
U-87 MG	Glioblastoma		WT	WT	WT	97.35

Figure 1

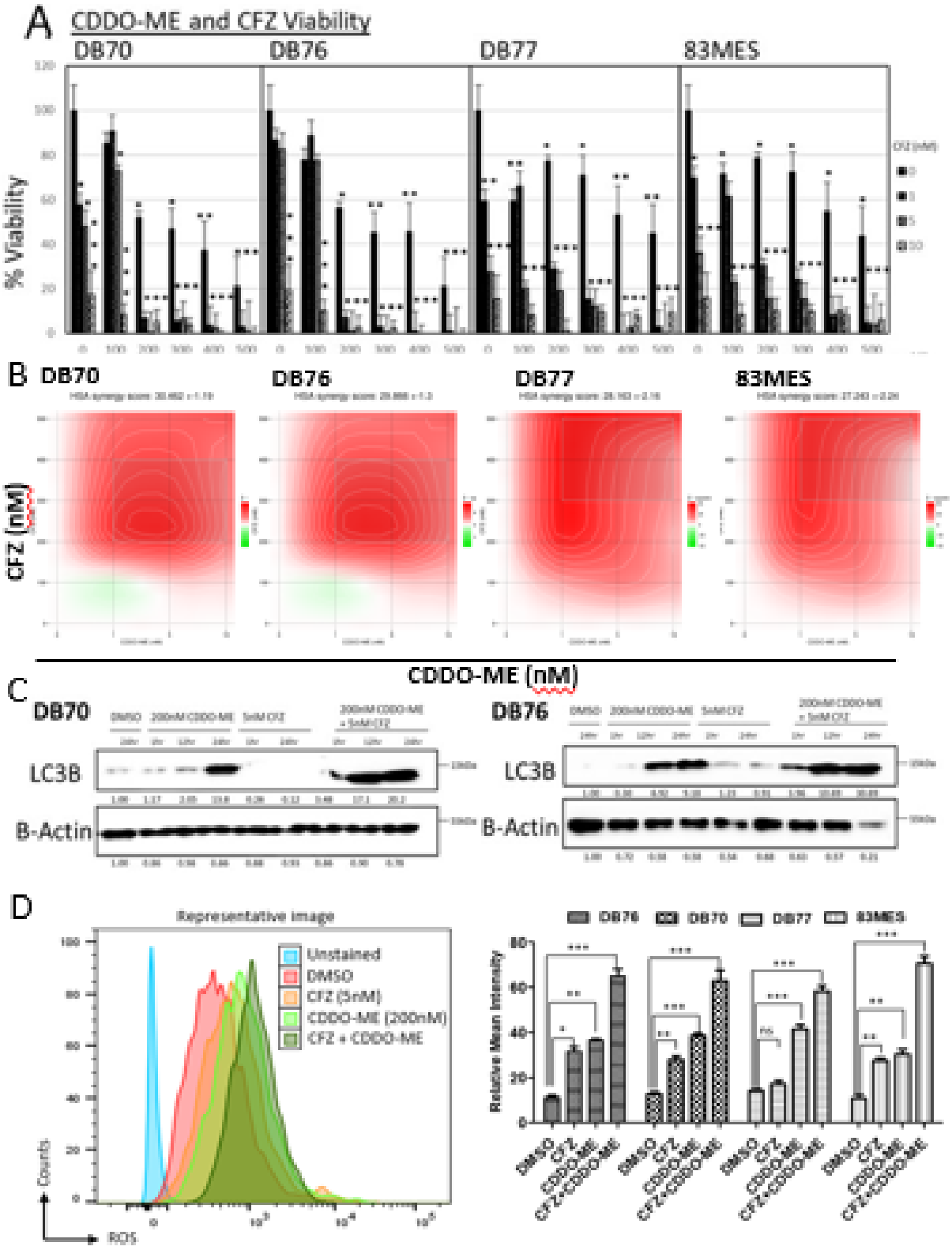
A
CDDO-ME and CFZ Viability
DB70
DB76
DB77
83MES
% Viability
CFZ (nM)
B
DB70
DB76
DB77
83MES
CFZ (nM)
CDDO-ME (nM)
C
DB70
DB76
LC3B
B-Actin
D
Representative image
Unstained
DMSO
CFZ (5nM)
CDDO-ME (200nM)
CFZ + CDDO-ME
Counts
ROS
DB76
DB70
DB77
83MES
Relative Mean Intensity
DMSO
CFZ
CDDO-ME
CFZ+CDDO-ME

Figure 2

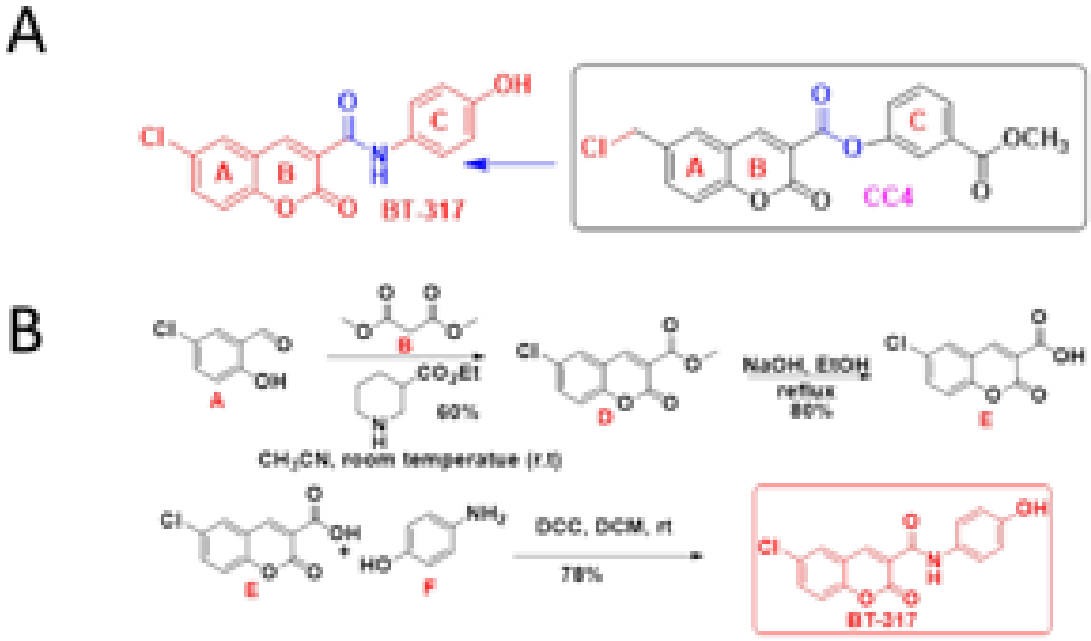

846

847

Figure 3

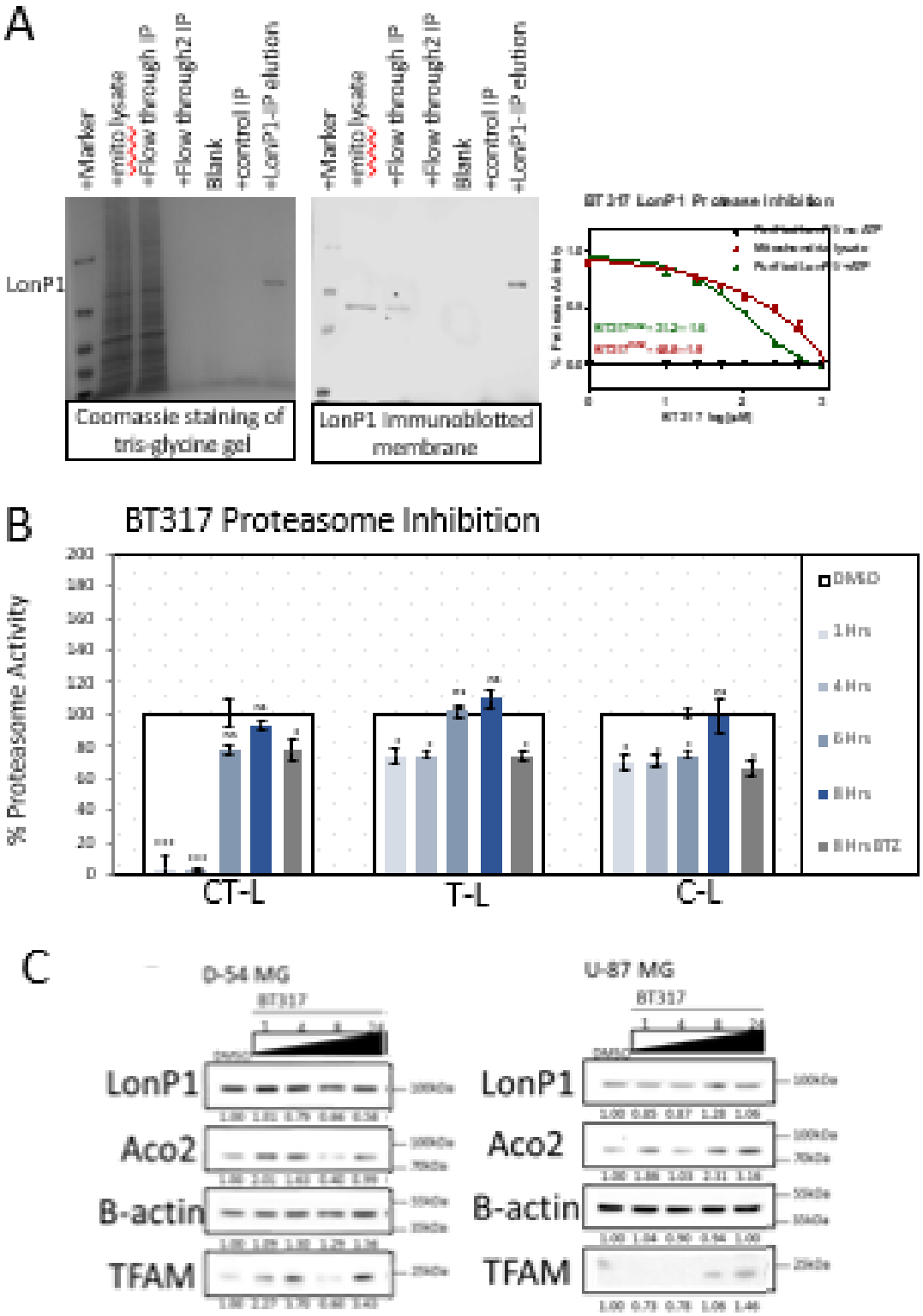

848

849

Figure 4

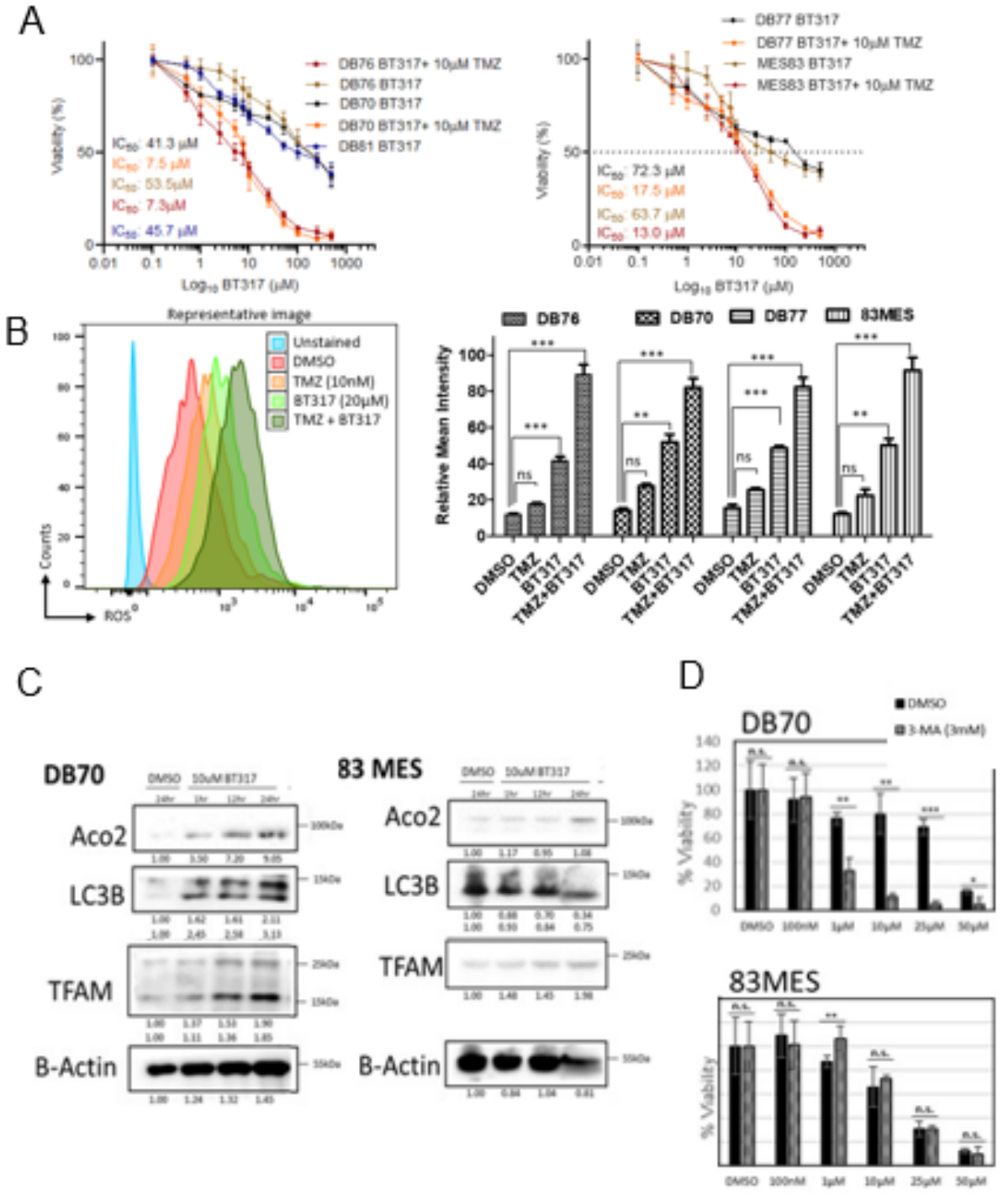

850

851

852

853

Figure 5

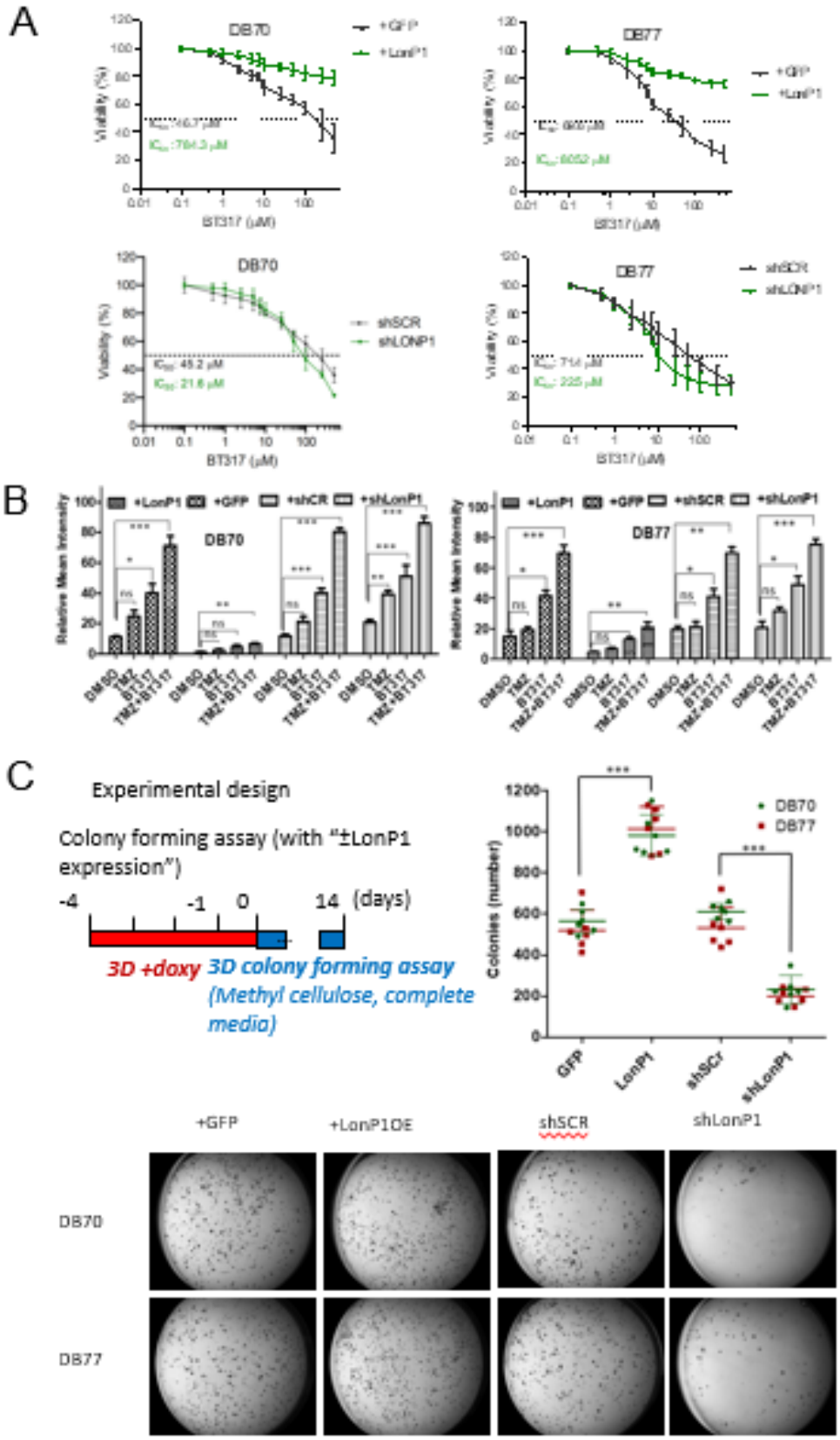
A
DB70
+GFP
+LonP1
Viability (%)
BT317 (µM)
DB77
shSCR
shLONP1
B
+LonP1
+GFP
+shCR
+shLonP1
Relative Mean Intensity
DMSO
TMZ
BT317
TMZ+BT317
C
Experimental design
Colony forming assay (with "±LonP1 expression")
-4
-1
0
14
(days)
3D +doxy
3D colony forming assay
(Methyl cellulose, complete media)
Colonies (number)
GFP
LonP1
shScr
shLonP1
+GFP
+LonP1OE
shSCR
shLonP1
DB70
DB77

Figure 6

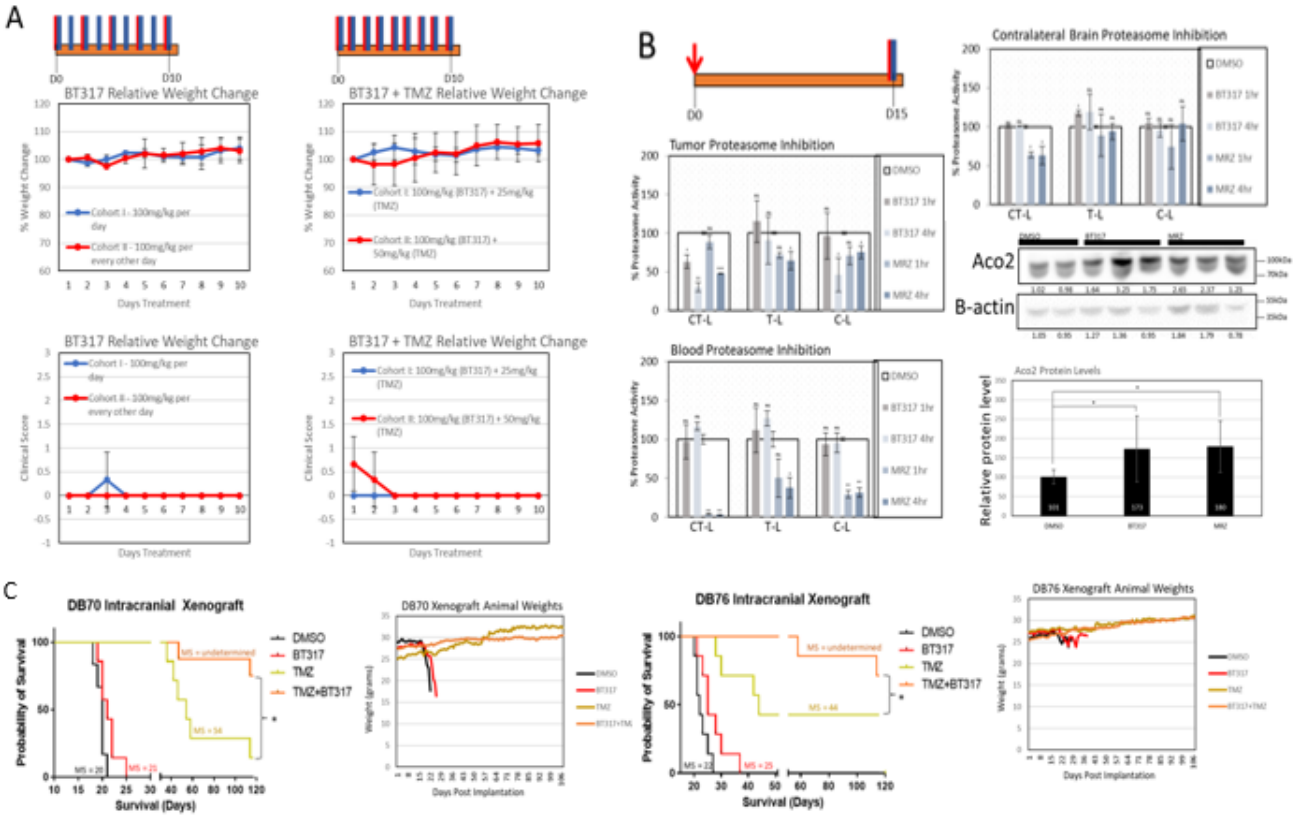
A
D0
D10
BT317 Relative Weight Change
% Weight Change
Cohort I - 100mg/kg per day
Cohort II - 100mg/kg per every other day
Days Treatment
BT317 + TMZ Relative Weight Change
Cohort I: 100mg/kg (BT317) + 25mg/kg (TMZ)
Cohort II: 100mg/kg (BT317) + 50mg/kg (TMZ)
Clinical Score
B
D0
D15
Tumor Proteasome Inhibition
Blood Proteasome Inhibition
Contralateral Brain Proteasome Inhibition
% Proteasome Activity
DMSO
BT317 1hr
BT317 4hr
MRZ 1hr
MRZ 4hr
CT-L
T-L
C-L
Aco2
B-actin
Aco2 Protein Levels
Relative protein level
C
DB70 Intracranial Xenograft
Probability of Survival
Survival (Days)
DMSO
BT317
TMZ
TMZ+BT317
MS = undetermined
MS = 54
MS = 25
DB70 Xenograft Animal Weights
Weight (grams)
Days Post Implantation
DB76 Intracranial Xenograft
MS = 44
MS = 23
DB76 Xenograft Animal Weights

855

Figure 1

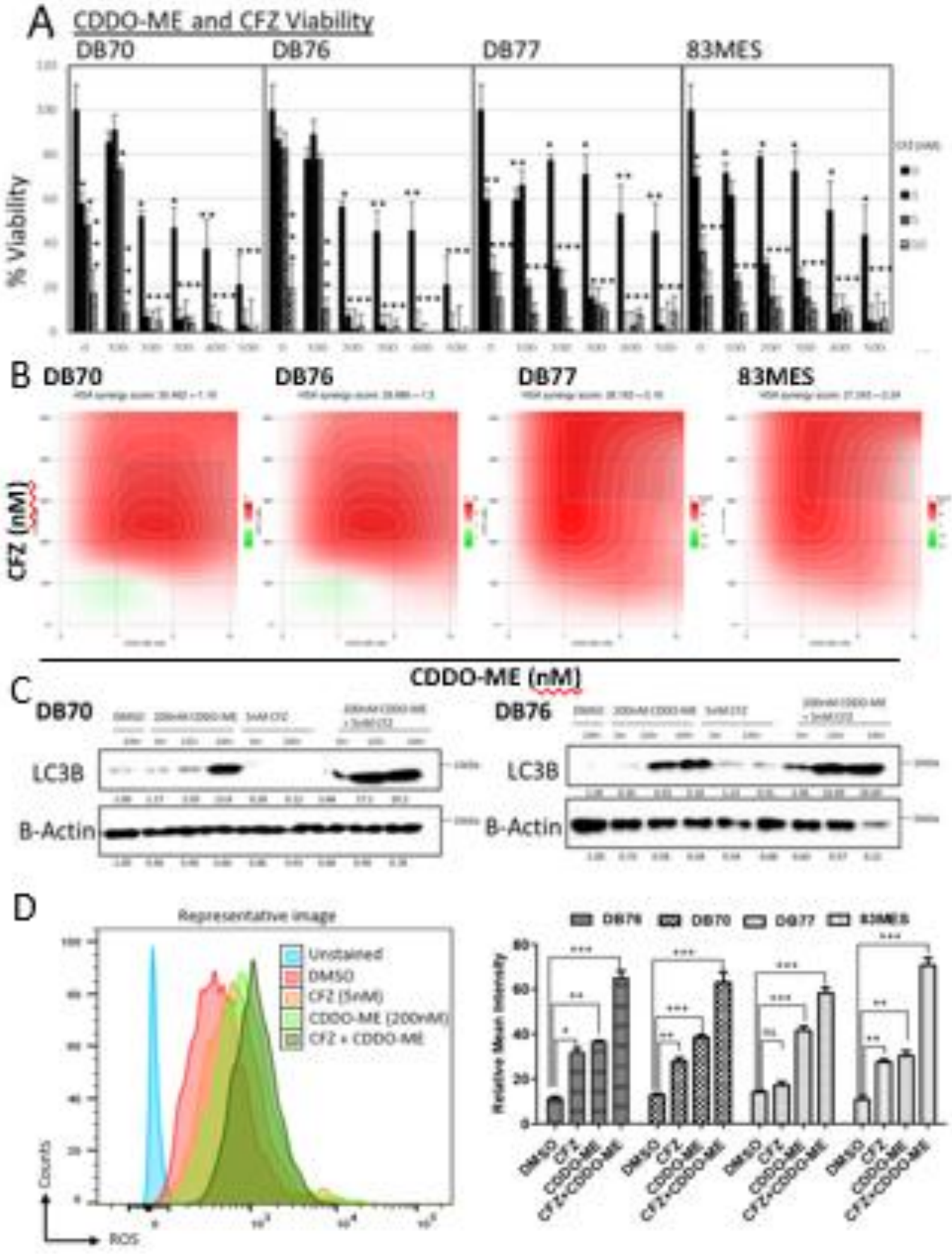
A
CDDO-ME and CFZ Viability
DB70
DB76
DB77
83MES
% Viability
B
DB70
DB76
DB77
83MES
CFZ (nM)
CDDO-ME (nM)
C
DB70
DB76
LC3B
B-Actin
D
Representative image
Unstained
DMSO
CFZ (5nM)
CDDO-ME (200nM)
CFZ + CDDO-ME
Counts
ROS
DB76
DB70
DB77
83MES
Relative Mean Intensity
DMSO
CFZ
CDDO-ME
CFZ+CDDO-ME

Figure 2

A

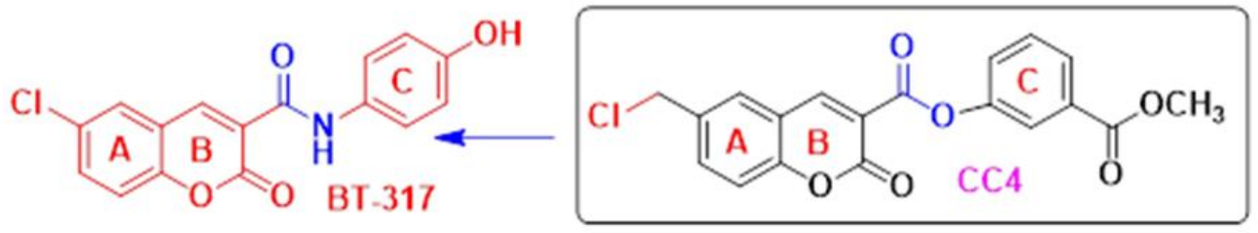
Cl
A
B
O
N
H
C
OH
BT-317
CC4
OCH3

B

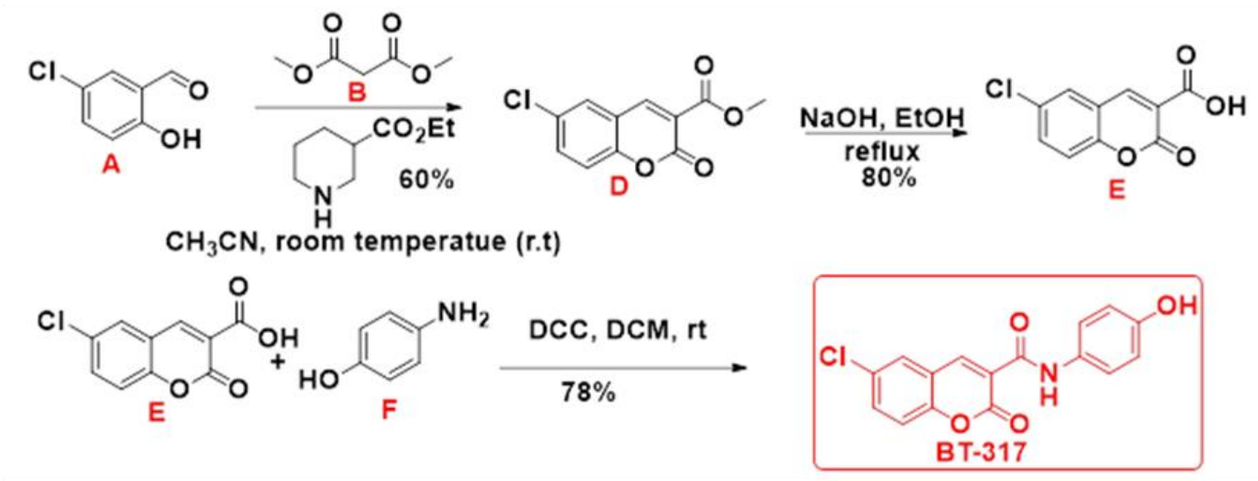
A
B
CO2Et
60%
CH3CN, room temperatue (r.t)
D
NaOH, EtOH
reflux
80%
E
F
DCC, DCM, rt
78%
BT-317

Figure 3

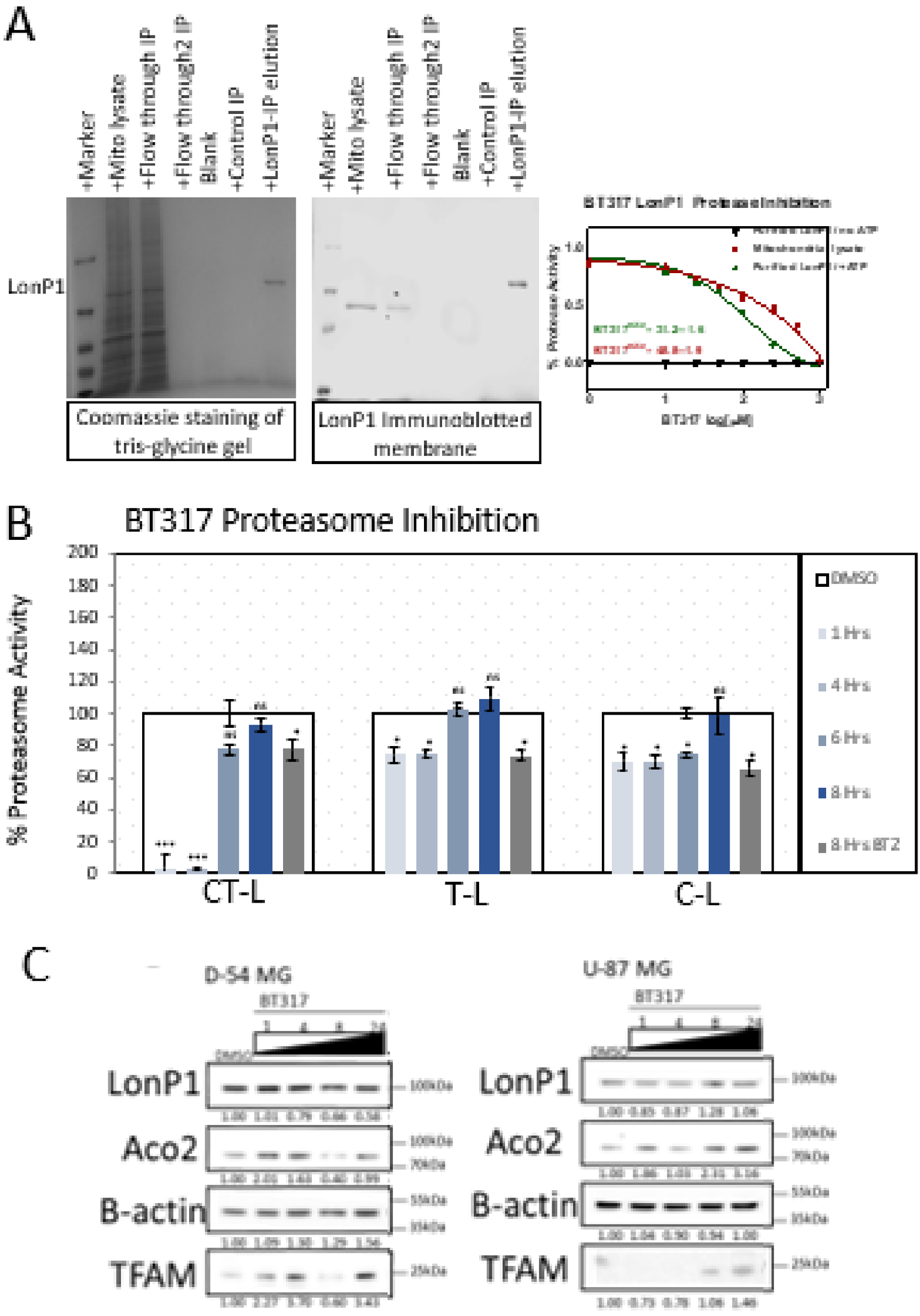
A
+Marker
+Mito lysate
+Flow through IP
+Flow through2 IP
Blank
+Control IP
+LonP1-IP elution
LonP1
Coomassie staining of tris-glycine gel
LonP1 Immunoblotted membrane
BT317 LonP1 Proteasome Inhibition
% Proteasome Activity
BT317 log[μM]
B
BT317 Proteasome Inhibition
% Proteasome Activity
CT-L
T-L
C-L
DMSO
1 Hrs
4 Hrs
6 Hrs
8 Hrs
8 Hrs BT2
C
D-54 MG
U-87 MG
BT317
DMSO
LonP1
Aco2
B-actin
TFAM

Figure 4

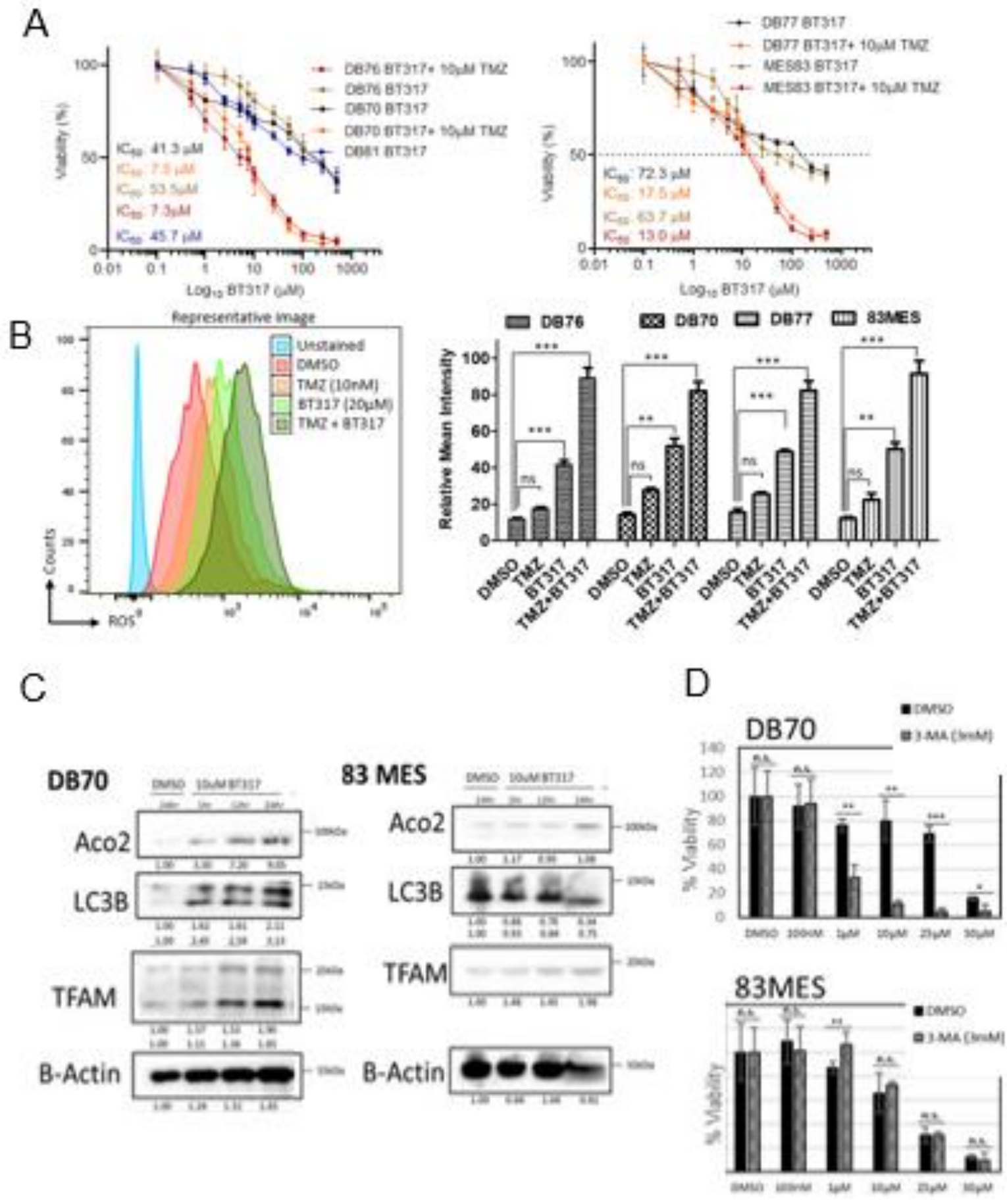
A
DB76 BT317+ 10μM TMZ
DB76 BT317
DB70 BT317
DB70 BT317+ 10μM TMZ
DB81 BT317
Viability (%)
Log10 BT317 (μM)
DB77 BT317
DB77 BT317+ 10μM TMZ
MES83 BT317
MES83 BT317+ 10μM TMZ
B
Representative image
Unstained
DMSO
TMZ (10nM)
BT317 (20μM)
TMZ + BT317
Counts
ROS
DB76
DB70
DB77
83MES
Relative Mean Intensity
DMSO
TMZ
BT317
TMZ+BT317
C
DB70
83 MES
Aco2
LC3B
TFAM
B-Actin
D
DB70
83MES
DMSO
3-MA (5mM)
% Viability

Figure 5

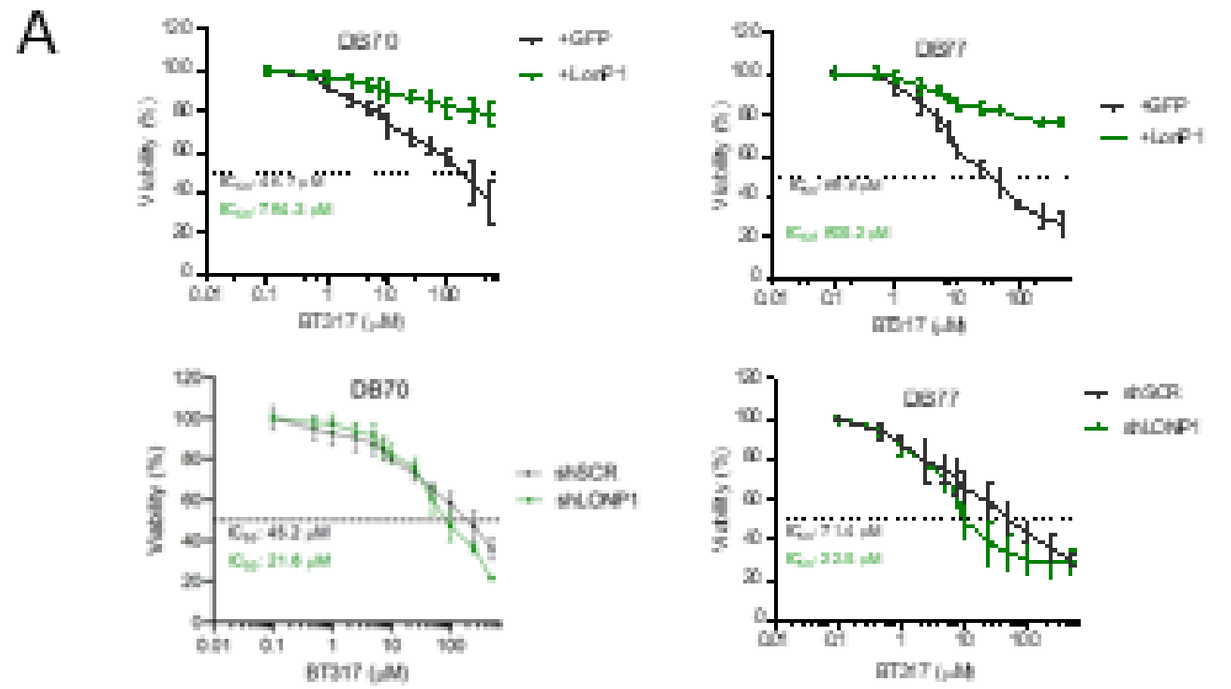
A
DB70
DB77
+GFP
+LonP1
shSCR
shLONP1
Viability (%)
BT317 (μM)

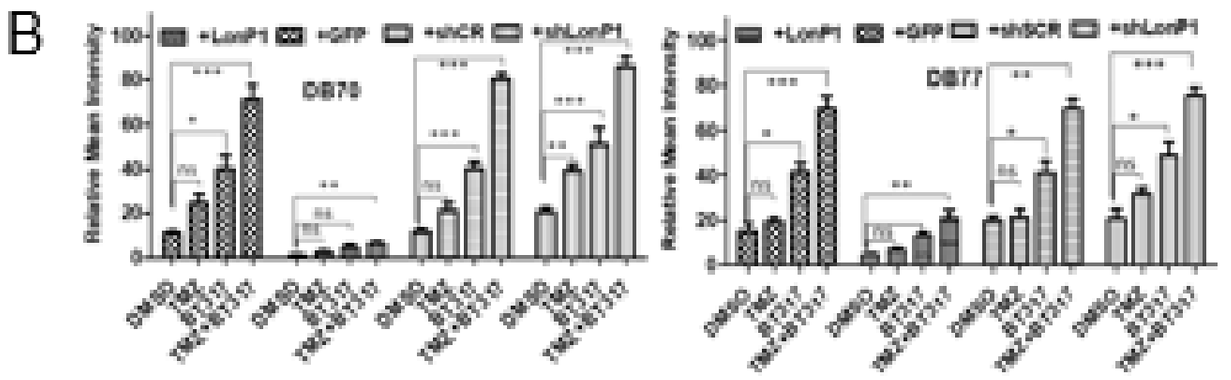
B
+LonP1
+GFP
+shSCR
+shLonP1
DB70
DB77
Relative Mean Intensity

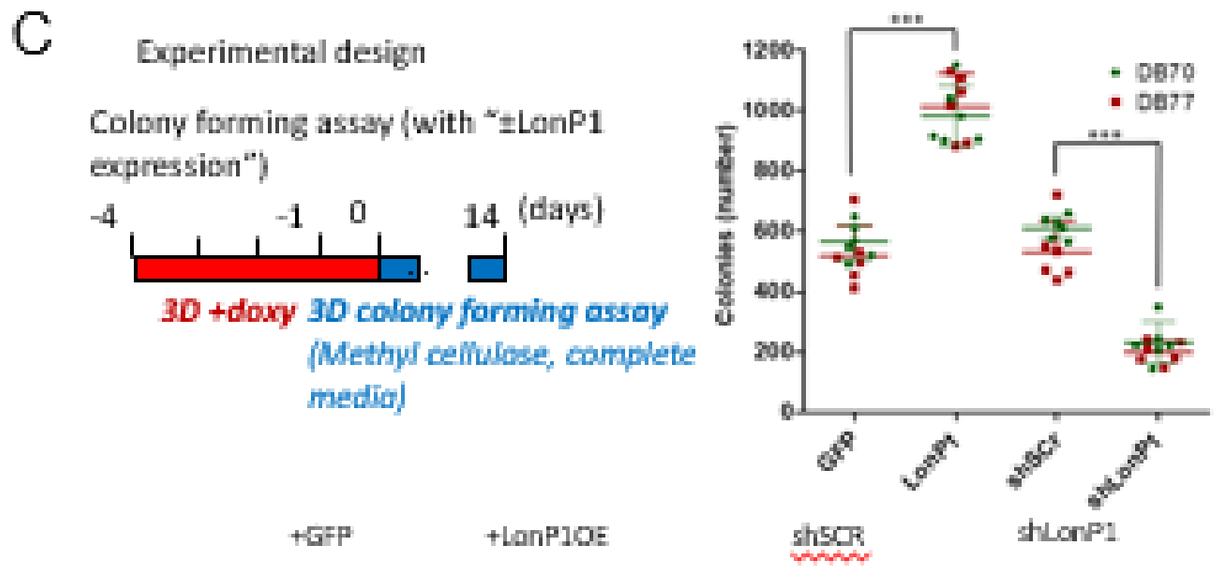
C
Experimental design
Colony forming assay (with "±LonP1 expression")
-4
-1
0
14
(days)
3D +doxy
3D colony forming assay
(Methyl cellulose, complete media)
DB70
DB77
Colonies (number)
GFP
LonP1
shSCR
shLonP1

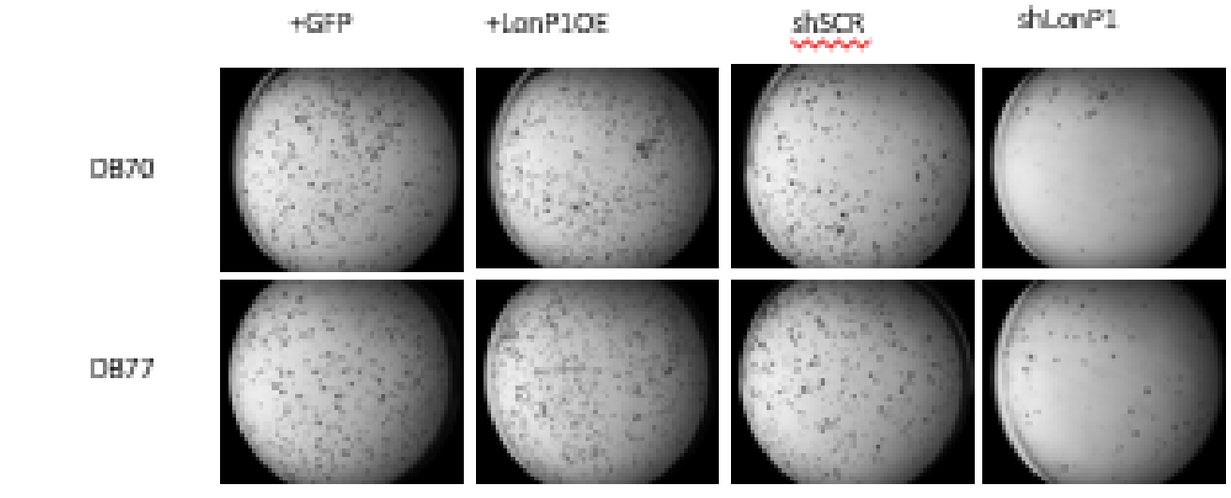
+GFP
+LonP1OE
shSCR
shLonP1
DB70
DB77

Figure 6

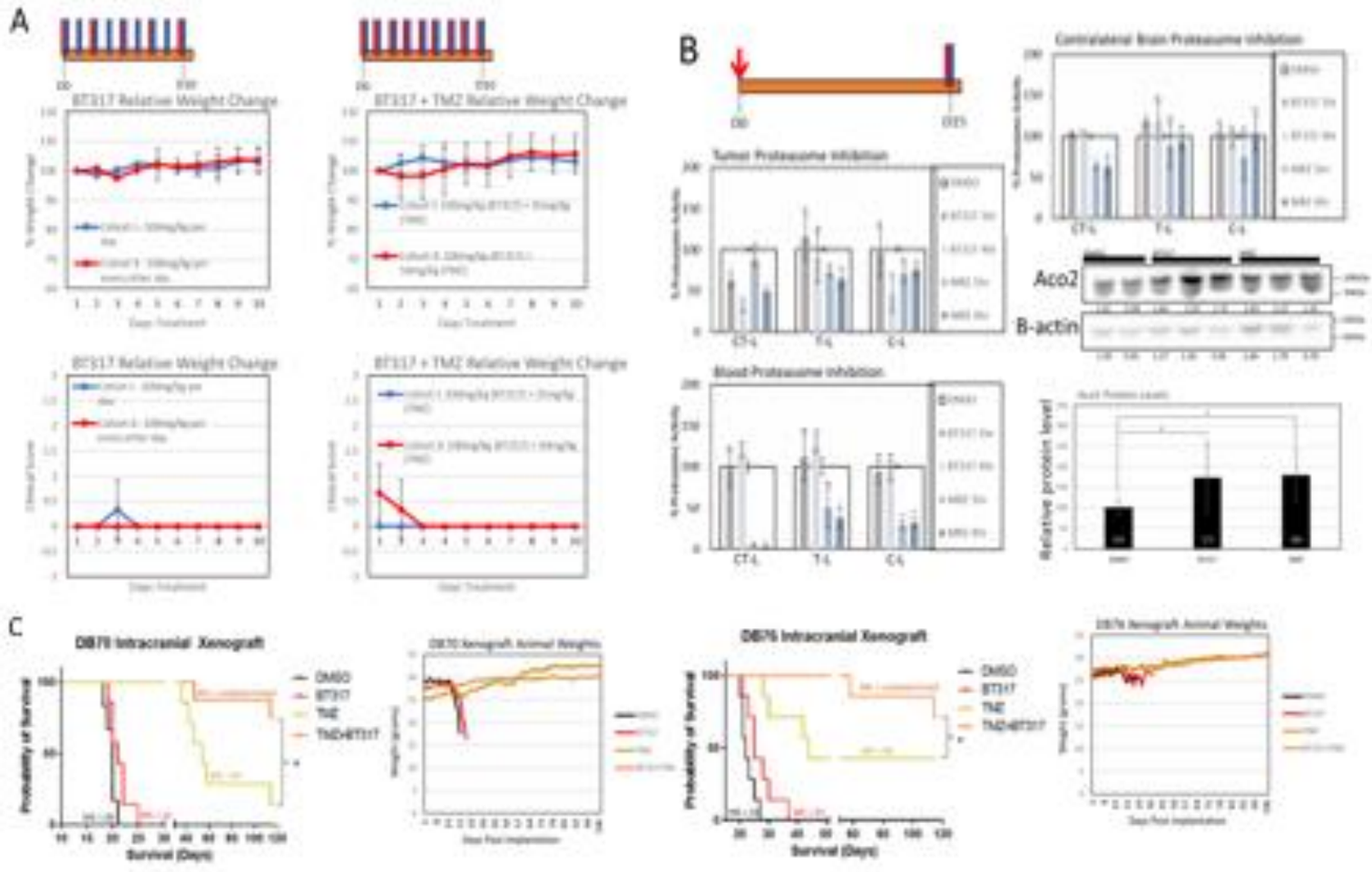
A
BT317 Relative Weight Change
BT317 + TMZ Relative Weight Change
B
Tumor Proteasome Inhibition
Contralateral Brain Proteasome Inhibition
Aco2
B-actin
Blood Proteasome Inhibition
Relative protein level
C
DB70 Intracranial Xenograft
DMSO
BT317
TMZ
TMZ+BT317
Survival (Days)
Probability of Survival